PLAXIS

PLAXIS 2024.1

User Defined Soil Model - BBM: Barcelona Basic Model in PLAXIS

Bentley®
Advancing Infrastructure

Last Updated: February 20, 2024

Table of Contents

1 Introduction

Unsaturated soils may be encountered in a wide variety of geotechnical engineering applications. They may constitute part of earth dams and embankments, and, in general, they characterise the soil layer close to the ground surface, which usually does not reach a state of complete saturation.

The behaviour of unsaturated soils cannot be fully captured by the classical models for fully saturated soils, since the presence of gas in the pores (e.g., air) together with water influences the properties and mechanical response of the soil.

In particular, the mechanical behaviour of unsaturated soils is strongly related to the concept of suction. Suction consists of two components: an osmotic and a matric suction. The former arises from the additional potential of the soil liquid due to the concentration of solute in the liquid phase, and is generally neglected in practical applications, while the latter is given by:

$$s = p_g - p_w \qquad Eq.\ [1]$$

where

p_g = Gas pressure.

p_w = Water pressure.

This has pushed for an increased interest in developing models capable of simulating the behaviour of unsaturated soils. Many constitutive models have been proposed in the past decades. Some of them are based on net stress (i.e., the excess of total stress over air pressure) and suction, as in the case of the famous Barcelona Basic Model proposed by Alonso et al. (1990) (on page 54). Other models have been developed considering Bishop's effective stress (Bishop, 1959; Bishop and Blight, 1963 (on page 54)) and suction as stress variables.

The PLAXIS Barcelona Basic Model (PLAXIS BBM), implemented as a User-Defined Soil Model in PLAXIS to simulate the behaviour of unsaturated soils, is based on the original BBM proposed by Alonso et al. (1990) (on page 54) with some differences and further developments. The main difference compared to the original formulation consists in the use of Bishop's effective stress, instead of net stress. Bishop's effective stress introduces a relationship between total stress, pore air pressure and pore water pressure but cannot describe alone the behaviour of unsaturated soils, as for example collapse due to wetting (Jennings and Burland, 1962 (on page 54)). That is why suction is generally needed to define the stress state of an unsaturated soil.

The advantage of the PLAXIS BBM formulation is the possibility to account for a smooth transition from a partially saturated state to a fully saturated condition, and vice versa, which is convenient for numerical modelling.

In the following, after highlighting the distinctive characteristics of the unsaturated soil behaviour, the constitutive equations describing the implementation of the PLAXIS BBM are presented, followed by a description of the model parameters and their calibration. The capability of the model to simulate the behaviour of unsaturated soils subjected to different loading and drainage conditions is discussed, together with the simulation of a practical engineering example in PLAXIS 2D.

1.1 The unsaturated soil behaviour

A summary of the main characteristics observed in unsaturated soils and that can be simulated using the PLAXIS BBM is presented hereafter.

Suction controlled experiments have shown that:

- An increase in suction results in:
  1. An increase in effective cohesion while maintaining the same value of the friction angle as in the fully saturated state(Fredlund et al., 1978 (on page 54); Alonso et al., 1990 (on page 54)), and an increase in preconsolidation stress (Dudley, 1970 (on page 54)).
- Changes in suction may induce both elastic and plastic volumetric strains, depending not only on the initial and final state but also on the stress path:
  1. A drying stress path is always characterised by compression of the soil sample.
  2. A wetting stress path may be characterised by either expansion (elastic swelling) or (plastic) collapse.
- At a certain value of suction, the slope of the normal compression line is different than the slope characterising the normal compression line at its fully saturated state.

Additionally, for both fully saturated and unsaturated soils, it is generally observed that the plastic strains may be described by a non-associated flow rule, and that the failure conditions cannot be well represented by a circular yield surface in the deviatoric plane. Therefore, a dependency of the yield and plastic potential surfaces on Lode's angle has been introduced in the PLAXIS BBM.

This model can be considered an extension of the Modified Cam-Clay model (Roscoe and Schofield, 1963 (on page 54); Schofield and Wroth, 1968 (on page 54)) not only for the possibility of simulating partial saturation but also for introducing the dependency from Lode's angle and a non-associated flow rule.

2 Constitutive equations

The PLAXIS BBM has been developed in the framework of Critical State Soil Mechanics and is based on the use of Bishop's effective stress and suction as stress variables.

Suction is described by Eq. [1]. It is generally assumed that the gas pressure p_g is equal to the atmospheric pressure p_a which is the zero-reference pressure level in PLAXIS. Therefore, the suction s is equal to $-p_w$.

Bishop's effective stress, which is used as a generalized Terzaghi's effective stress for unsaturated soil in PLAXIS, is given by:

$$\boldsymbol{\sigma}' = \boldsymbol{\sigma} - \boldsymbol{m}[\chi p_w + (1-\chi)p_a] \quad Eq.\ [2]$$

where

$\boldsymbol{\sigma}'$	=	Effective stress tensor.
$\boldsymbol{\sigma}$	=	Total stress tensor.
$\boldsymbol{m}$	=	Second order identity tensor.
p_w	=	Pore water pressure.
p_a	=	Pore air pressure.
χ	=	Matric suction coefficient, ranging from zero for dry soils to 1 for fully saturated soils.

Several attempts have been made to quantify χ (Bolzon et al., 1996 (on page 54), Khalili and Khabbaz, 1998 (on page 54)). In PLAXIS, it is assumed that $\chi = S_{eff}$, defined by:

$$S_{eff} = \frac{S - S_{res}}{S_{sat} - S_{res}} \quad Eq.\ [3]$$

The effective saturation S_{eff} depends on the degree of saturation S, the residual degree of saturation S_{res}, and S_{sat} at full saturation, generally set to 1.

Therefore, Bishop's effective stress can be written as:

$$\boldsymbol{\sigma}' = \boldsymbol{\sigma} - \boldsymbol{m}p_{active} \quad Eq.\ [4]$$

where:

$$p_{active} = S_{eff}\, p_w \quad Eq.\ [5]$$

To describe the hydraulic behaviour of the material in the unsaturated zone, the most common hydraulic model used in the groundwater literature relates the saturation S to the pressure head ψ (Van Genuchten, 1980 (on page 54), Mualem, 1976 (on page 54)):

$$S(\psi) = S_{res} + (S_{sat} - S_{res})\left[1 + (g_a \mid \psi \mid)^{g_n}\right]^{g_c} \quad Eq.\ [6]$$

with the pressure head ψ given by

$$\psi = -\frac{p_w}{\gamma_w} \qquad Eq.\ [7]$$

where

γ_w = Unit weight of water.

The parameters g_a, g_n and g_c are fitting parameters, with g_c equal to:

$$g_c = \frac{1 - g_n}{g_n} \quad Eq.\ [8]$$

More details can be found in Chapter: **Hydraulic Models** of the PLAXIS Material Model Manual.

2.1 Elastic response

As in the classical elasto-plasticity theory, the total strain rate tensor can be decomposed into an elastic and a plastic part as shown in Eq. [9]:

$$\dot{\boldsymbol{\varepsilon}} = \dot{\boldsymbol{\varepsilon}}^e + \dot{\boldsymbol{\varepsilon}}^p \quad Eq.\ [9]$$

Within the elastic region, the elastic response is assumed to be isotropic and defined by the bulk stiffness K depending linearly on the mean effective pressure, the shear stiffness G calculated as a function of the bulk modulus and a constant coefficient of Poisson ν', and the stiffness K_s depending on suction:

$$K = \frac{v\,p'}{\kappa} \quad Eq.\ [10]$$

$$G = \frac{3\left(1 - 2\nu'\right)}{2\left(1 + \nu'\right)}K \quad Eq.\ [11]$$

$$K_s = \frac{v\left(s + p_a\right)}{\kappa_s} \quad Eq.\ [12]$$

where

v = Specific volume, equal to $\left(1 + e_0\right)$, with e_0 as the initial void ratio at a reference effective pressure p_r.

κ = Slope of the swelling line in the $\left(v,\ ln\ p'\right)$ plane.

κ_s = Slope of the swelling line in the $\left(v,\ ln\ s\right)$ plane.

p_a = Atmospheric pressure.

Both changes in effective stresses and in suction generates elastic volumetric strains, such that the strain increment is:

$$\dot{\varepsilon}_v^e = \frac{\kappa}{1 + e_0}\frac{\dot{p}'}{p'} + \frac{\kappa_s}{1 + e_0}\frac{\dot{s}}{s + p_a} \qquad Eq.\ [13]$$

while the elastic deviatoric strain increment is calculated as:

$$\dot{\varepsilon}_q^e = \frac{\dot{q}}{3G} \qquad Eq.\ [14]$$

At constant suction $(\dot{s} = 0)$, the elastic behaviour is equivalent to the one predicted by the Modified Cam-Clay model.

2.2 Yield surface

The model is characterised in an extended stress space (p', q, s). At a given suction, the yield surface in the (p', q) plane is an elliptical yield surface centred along the isotropic axis. A representation of the model surfaces in the (p', q) plane is shown in Figure 1 (on page 7). One surface represents the yield function for a fully saturated sample $(s = 0)$, the other one has the same shape but is proportionally larger based on the current suction value and represents the yield surface for the unsaturated case. Note that, the behaviour inside the yield surface is purely elastic.

At full saturation, the surface passes from the origin of the stress space and is defined by p_0', i.e. the mean effective preconsolidation pressure. For increasing values of suction, the yield surface expands along both the negative and the positive side of the isotropic axis.

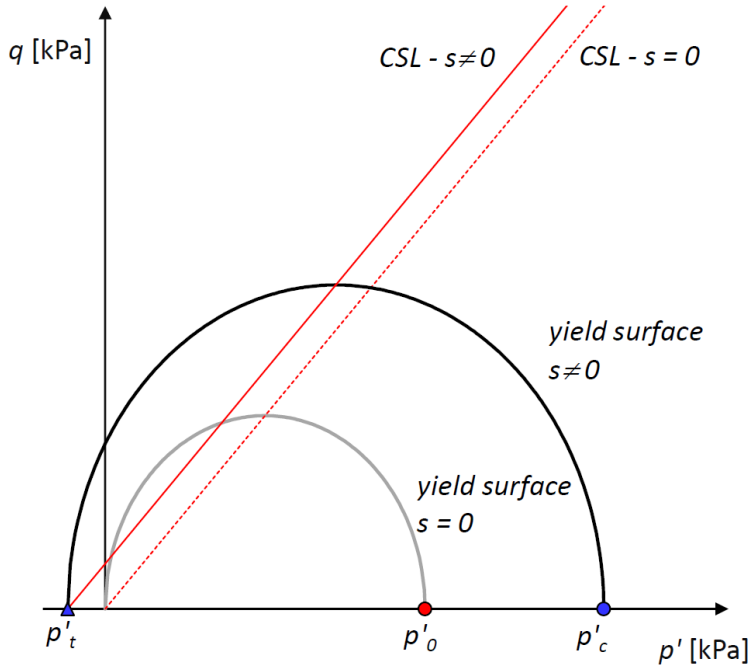

Figure 1: BBM model surfaces

The yield surface is described by the following relationship:

$$f = 3J^2 - \left(\frac{g(\theta)}{g(-1)}\right)^2 M^2 (p' + p_t')(p_c' - p') \qquad Eq.\ [15]$$

where

$J = \sqrt{J_2} = \sqrt{\frac{1}{2}\mathbf{s} : \mathbf{s}} = q \,/\, \sqrt{3}$ = with J_2 being the second invariant of the deviatoric tensor $\mathbf{s}$.

M = Stress ratio at critical state at full saturation for compressive triaxial stress state, determined by the friction angle φ according to :

$$M = \frac{6\sin\varphi}{3 - \sin\varphi} \quad Eq.\ [16]$$

where

$p_t{}'$ = Intersection of the yield surface on the negative side of the mean pressure axis, which represents a tensile strength due to suction equal to

$$p_t{}' = k_s s \quad Eq.\ [17]$$

where

$p_c{}'$ = Preconsolidation pressure at unsaturated state, which will be described later.

$g(\theta)$ defines the yield response in the deviatoric plane and, according to Sheng et al. (2000) (on page 54), is equal to:

$$g(\theta) = \left(\frac{2\alpha_\varphi}{1 + \alpha_\varphi + (1 - \alpha_\varphi)\sin(3\theta)}\right)^{\frac{1}{4}} \quad Eq.\ [18]$$

with α_φ being a function of the friction angle φ:

$$\alpha_\varphi = \left(\frac{3 - \sin\varphi}{3 + \sin\varphi}\right)^4 \quad Eq.\ [19]$$

A dependency on Lode's angle θ is accounted for through the second and third invariant of the deviatoric tensor, J_2 and J_3 $\left(J_3 = det\ (\mathbf{s})\right)$:

$$\sin(3\theta) = -\left(\frac{3\sqrt{3}}{2}\frac{J_3}{J_2^{3/2}}\right) \quad Eq.\ [20]$$

The introduction of $g(\theta)$ represents an improvement with respect to both the Modified Cam-Clay model and the original implementation of BBM, since it introduces the dependency on Lode's angle θ, avoiding strength overestimation in extension, and potential convergence issues at the corner points (Figure 2 (on page 9)). It is important to note that the yield function in the deviatoric plane closely approximates the well-known Matsuoka-Nakai's yield contour (Pedroso and Farias, 2011 (on page 54)).

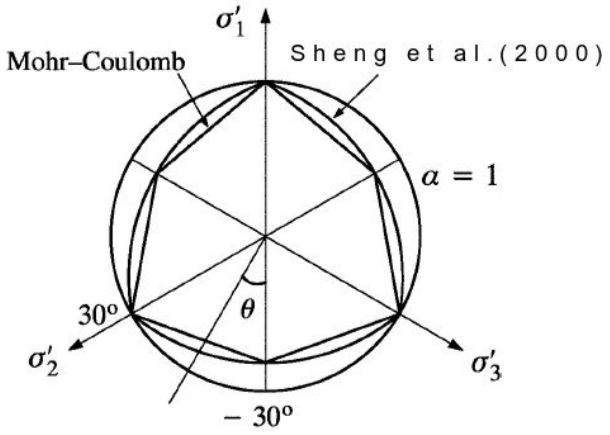

Figure 2: Model surface in the deviatoric plane: Mohr-Coulomb, Modified Cam-Clay ($\alpha = 1$) and Sheng et al. (2000), adapted from Sheng et al. (2000)

The relationship between $p_0{}'$ and $p_c{}'$ is given by Eq. [21]:

$$\left(\frac{p_c{}'}{p_r}\right) = \left(\frac{p_0{}'}{p_r}\right)^{\frac{\lambda_0 - \kappa}{\lambda(s) - \kappa}} \qquad Eq.\ [21]$$

where

λ = Slope of the isotropic compression line in the $(v,\ ln\ p')$ plane.

More precisely, λ_0 describes the fully saturated case, while $\lambda(s)$ refers to a specific value of suction s:

$$\lambda(s) = \lambda_0\left[(1 - r)e^{(-\beta s)} + r\right] \qquad Eq.\ [22]$$

The parameters r and β define the shape of the loading-collapse curve (LC) which delimits the elastic region in the $(p',\ s)$ stress plane (Figure 3 (on page 10)), as it will be discussed in Model initialisation and yield surface parameters (on page 13).

A correct calibration of the parameters r, β and p_r can ensure that the shape of the LC curve is such that it simulates an increase in preconsolidation pressure with increasing suction and, therefore, a larger ellipse in the $(p',\ q)$ plane. However, in practical situations, the unsaturated preconsolidation $p_c{}'$ calculated using Eq. [21], can be lower than $p_0{}'$, leading to an unexpected softening behaviour with suction. This also happens with the original BBM . Therefore, in this PLAXIS BBM version, a strategy has been implemented to prevent the unrealistic prediction of decreased strength with increasing suction, as shown in Figure 4 (on page 10). In fact, $p_c{}'$ is bound to be at least equal to $p_0{}'$ resulting from Eq. [21] .

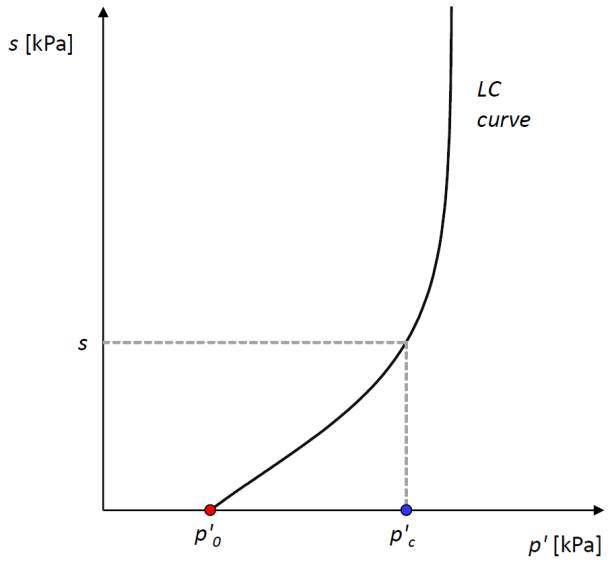

Figure 3: Loading-collapse curve in the (p', s) plane

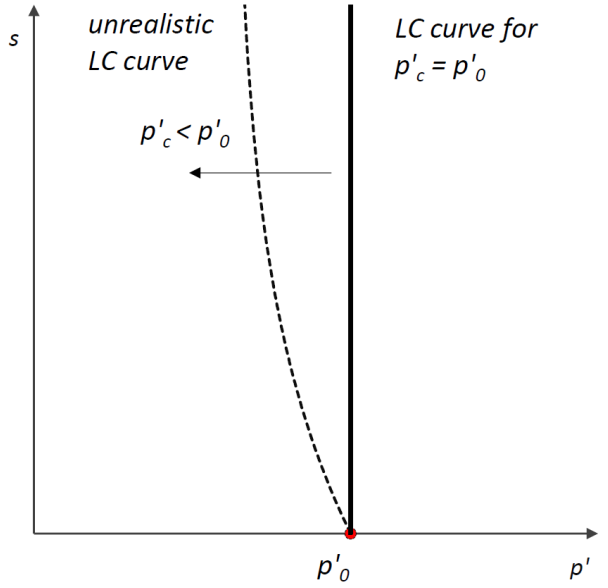

Figure 4: Representation of LC curve assumption when the calculated p_c' is not larger than p_0'

A representation of the model in the three-dimensional space is shown in Figure 5 (on page 11).

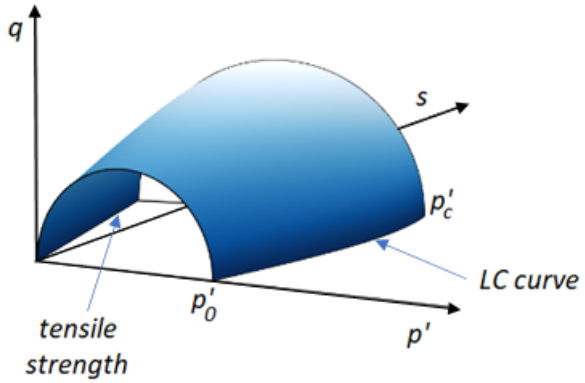

Figure 5: Three-dimensional representation of the PLAXIS BBM model surfaces

2.3 Flow rule

The equation of the plastic potential is similar to the one of the yield function, with the addition of the parameter α (Ohmaki, 1982 (on page 54)), larger than zero as shown in Eq. [23]:

$$g = 3\alpha J^2 - \left(\frac{g(\theta)}{g(-1)}\right)^2 M^2 (p' + p_t')(p_c' - p') \qquad Eq.\ [23]$$

When α is equal to 1, the two surfaces coincide, meaning that the flow rule is associated as in Modified Cam-Clay. Therefore, the vector of the plastic strain increment is perpendicular to the yield surface at the current stress state.

However, a non-associated flow rule can be accounted for by setting α different than 1, which results in a different shape of the plastic potential g and, therefore, a different inclination of the plastic strain increment vector, as shown in Figure 6 (on page 12) for α equal to 0.474. In terms of predicted soil behaviour, for the same stress state, larger plastic volumetric strains are predicted when α is 0.474, compared to the associated flow rule.

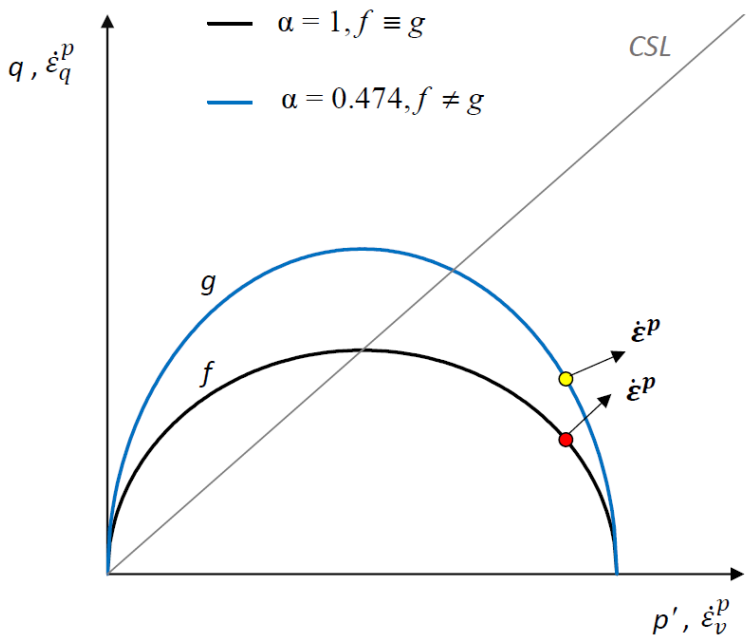

Figure 6: Representation of the yield surface and two plastic potential functions for associated and non-associated flow rule, with the indication of the plastic strain increment vector

2.4 Hardening rule

The model surfaces evolve together with p_0' and s according to two volumetric isotropic hardening rules:

$$\dot{p}'_0 = \frac{v\dot{\varepsilon}_v^p}{\lambda_0 - \kappa} p_0' \quad \textit{Eq. [24]}$$

$$\dot{s} = \frac{v\dot{\varepsilon}_v^p}{\lambda(s) - \kappa_s}(s + p_{atm}) \quad \textit{Eq. [25]}$$

Due to Eq. [21], a change in p_0' also determines an evolution of p_c'. The predicted behaviour could be either compressive (on the wet side of critical state) or dilatant (on the dry side of critical state) (Roscoe et al., 1958 (on page 54)).

3 Model input and state parameters

The parameters characterising the PLAXIS BBM and the corresponding calibration strategy are described in the next paragraphs, together with the state parameters available in PLAXIS for this model.

3.1 Model initialisation and yield surface parameters

The input parameters that are needed to initialise the model surface in PLAXIS are summarised in Table 1 (on page 13). Most of these parameters can be determined through conventional laboratory or in-situ tests, while others need to be calibrated according to the desired behaviour.

Table 1: PLAXIS BBM input parameters for model initialisation and for the yield surface

Symbol	Description	Unit	Range of validity
k_s	Factor accounting for tensile strength due to suction	-	≥0
φ	Friction angle at critical state	o	$0 < \varphi < 89$
λ	Slope of the compression line of the fully saturated material, in the (v, $ln\ p'$) plane	-	> κ
p_r	Reference effective pressure	kPa	>0
r	Parameter controlling the soil stiffness with suction	-	>0
β	Parameter controlling the rate of increase of soil stiffness with suction	kPa^{-1}	>0

Symbol	Description	Unit	Range of validity
$k0_{NC}$	Coefficient of earth pressure at rest in normal consolidation	-	>0
OCR	Overconsolidation ratio	-	≥1
POP	Pre-Overburden pressure	kPa	≥0

The yield surface is represented by an ellipse in the (p', q) plane and by the loading-collapse curve (LC curve), in the (p', s) plane.

The yield function associated to a specific stress state is defined by p_t', p_c' and M, in the (p', q) plane. These quantities are derived based on:

- Eq. [16], in the case of M, depending on φ only.
- Eq. [17], in the case of p_t', depending on the factor k_s for an initial suction given as input in the simulation of laboratory tests using SoilTest or based on the groundwater flow boundary conditions for the simulation of boundary value problems.
- Eq. [15], in the case of p_c', where, in addition to the previous quantities, the current stress state is needed, calculated based on K_0^{NC} and either OCR or POP:

$$p_c' = 3J^2\left(\frac{g(-1)}{g(\theta)}\right)^2 \frac{1}{M^2\left(p' + p_t'\right)} + p' \qquad Eq.\ [26]$$

where

$$p' = \frac{\left(\sigma_v' - POP\right)\left(1 + 2k_0^{NC}\right)}{3} \quad when\ \ OCR < 1 \qquad Eq.\ [27]$$

$$p' = \frac{\left(\sigma_v'\ OCR\right)\left(1 + 2k_0^{NC}\right)}{3} \quad when\ \ OCR \geq 1 \qquad Eq.\ [28]$$

where

σ_v' = Effective vertical stress.

The value of k_s can be determined considering the increase in the stress ratio at critical state measured at a specific value of suction, and the contribution of suction to the soil tensile strength, e.g.:

$$k_s = \frac{q - q_{FS}}{Ms} \qquad Eq.\ [29]$$

where

q = Shear strength at critical state for a given value of suction s.
q_{FS} = Shear strength at critical state at full saturation.

When no other measurements are available, the friction angle could be used to determine K_0^{NC} (Jaky, 1944 (on page 54)):

$$K_0^{NC} = 1 - \sin\varphi \qquad Eq.\ [30]$$

The yield surface is represented by the loading-collapse curve (LC curve) in the (p', s) plane, which describes the evolution of the preconsolidation pressure with suction, starting from p_0' at the fully saturated state, which is calculated based on Eq. [21] and the value of p_c' obtained during the model initialisation.

The slope of the compression line λ can be determined based on the results of one-dimensional or isotropic compression tests on fully saturated samples. The remaining parameters p_r, r and β, should be calibrated to achieve the desired evolution of p_c' with suction.

In general, for sufficiently small values of p_r, r must be a positive value lower than 1. However, the strategy described in paragraph Yield surface (on page 7) always ensures that p_c' is larger than or equal to p_0'. As for the lower bound of r, it is recommended to set r larger than κ / λ_0 (Pereira, 2011 (on page 54)) but also to graphically represent the LC curve. As shown in Figure 7 (on page 15), in this case, r equal to κ / λ_0 corresponds to an extremely large yield surface at small values of suction. The effect of the variation of β is shown in Figure 8 (on page 16). When r is equal to 1 or β is equal to 0, λ_s is equal to λ_0 and, therefore p_c' is equal to p_0'.

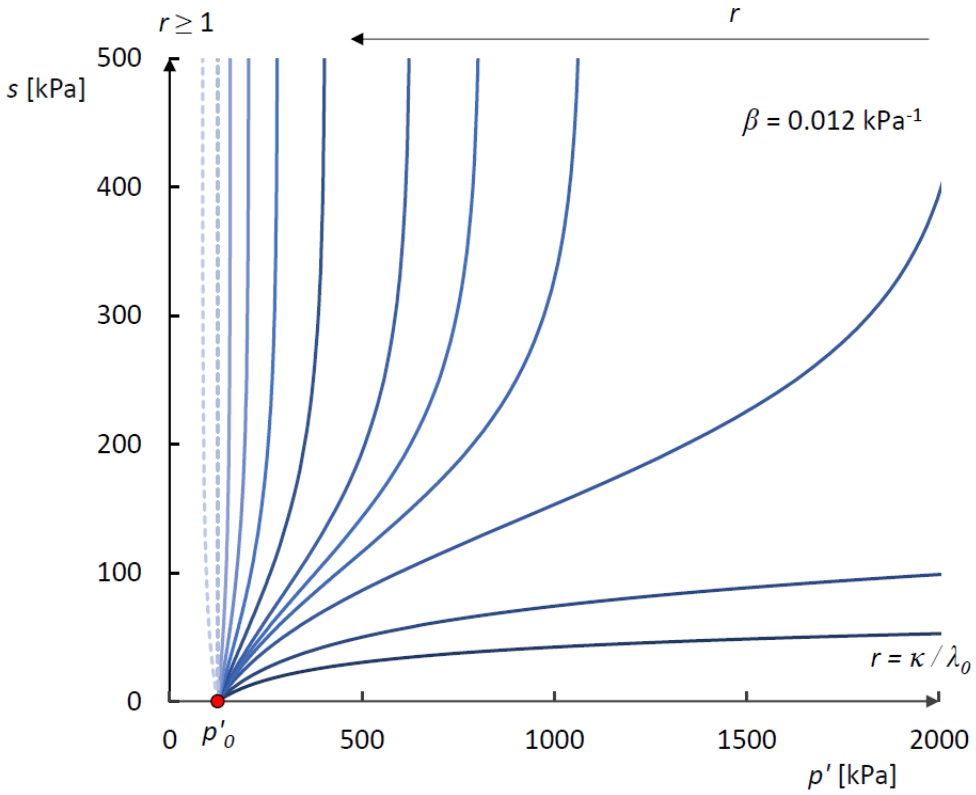

Figure 7: LC curve for different values of r and β equal to 0.012 kPa^{-1}

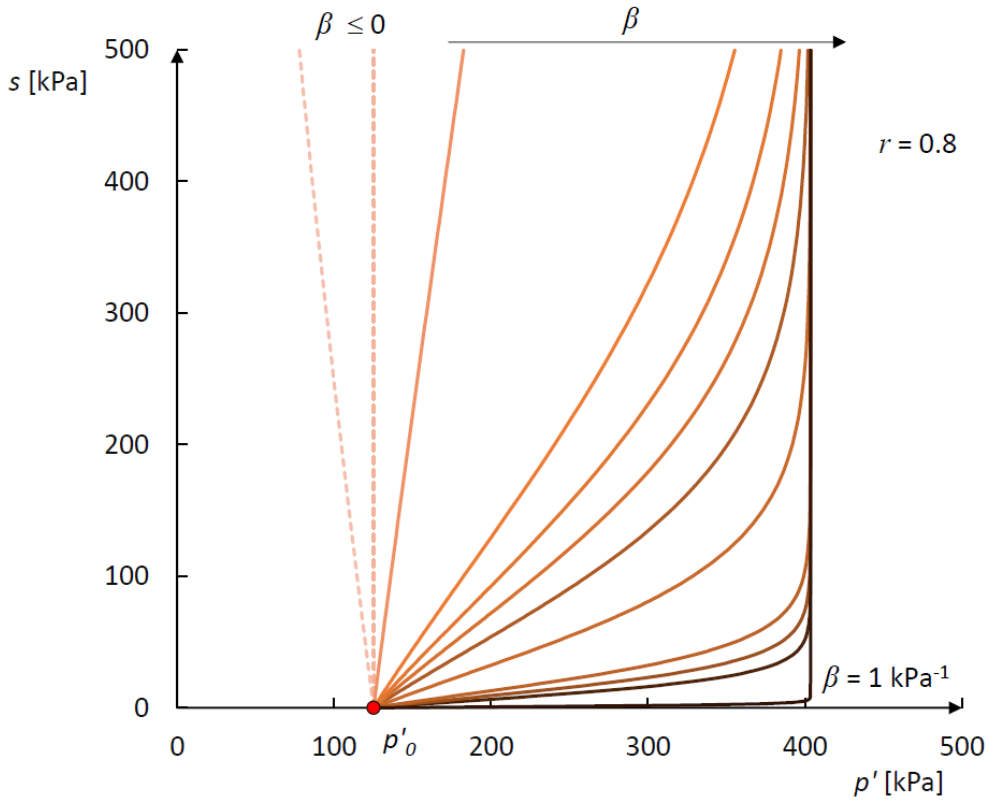

Figure 8: LC curve for different values of β and r equal to 0.8

3.2 Elastic parameters

The elastic behaviour associated to a change in both stresses and suction is defined by Eq. [13] and Eq. [14], and depends on the input parameters in Table 2 (on page 16):

Table 2: PLAXIS BBM parameters for the elastic state

Symbol	Description	Unit	Range of validity
ν'	Poisson's ratio	-	$0 < \nu' < 0.499$
κ	Slope of the swelling line in the $(v,\ ln\ p')$ plane	-	> 0
κ_s	Slope of the swelling line in the $(v,\ ln\ s)$ plane	-	≥0
e_0	Initial void ratio	-	>0

The swelling parameter κ can be determined based on one-dimensional or isotropic compression tests on fully saturated samples, during which at least one unloading stress path has been performed.

The swelling parameter κ_s describes the elastic response to a change in suction and can be determined indirectly performing an elastic drying or wetting path at constant total stress. However, it should be taken into consideration that the slope of the swelling line in that case is also partially influenced by κ, since a change in suction is always associated to a change in effective stresses. Integrating the elastic volumetric strain increment (Eq. [13]) between two suction values, s_1 and s_2, it is possible to write:

$$\Delta v - \kappa \ln \frac{p_2'}{p_1'} = \frac{\kappa_s}{s_1 + p_a}(s_2 - s_1) \qquad \textit{Eq. [31]}$$

Which allows to calculate κ_s as:

$$\kappa_s = \left(\Delta v - \kappa \ln \frac{p_2'}{p_1'} \right) \frac{(s_1 + p_a)}{(s_2 - s_1)} \qquad \textit{Eq. [32]}$$

The swelling parameters are represented in Figure 9 (on page 17), and they can be transformed into the modified swelling indices κ^* and κ_s^*.

$$\kappa^* = \frac{\kappa}{1 + e_0} \qquad \textit{Eq. [33]}$$

$$\kappa_s^* = \frac{\kappa_s}{1 + e_0} \qquad \textit{Eq. [34]}$$

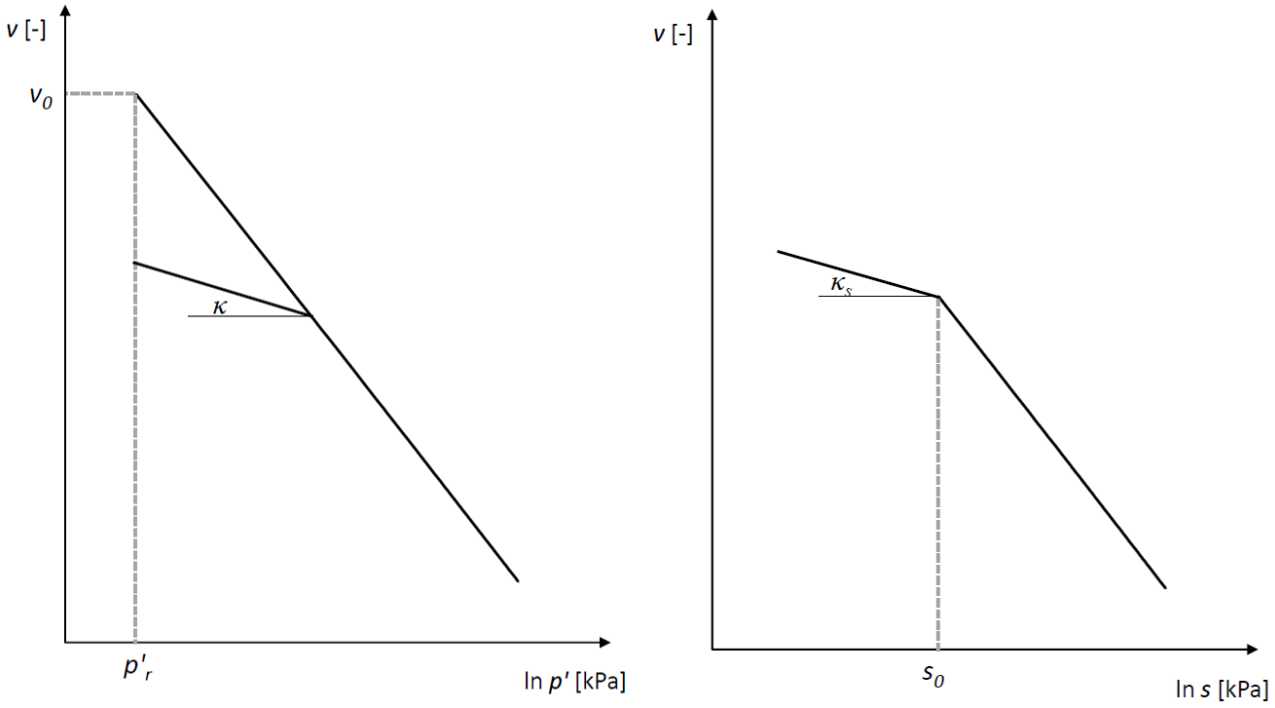

Figure 9: Representation of the stiffness parameters in the corresponding semi-log plane

3.3 Plastic potential

As described in paragraph Flow rule (on page 11), the plastic potential function g is defined by the same parameters as the yield function f, with the additional α parameter (Table 3 (on page 18)).

Table 3: PLAXIS BBM parameters for the plastic potential

Symbol	Description	Range of validity	Unit
α	Coefficient of the plastic potential	>0	-

When a non-associated flow rule better represents the material behaviour, the value of α can be set to a value different than 1. The shape of the plastic potential function can be indirectly determined based on triaxial tests results. However, Alonso et al. (1990) (on page 54) proposed Eq. [35] for calculating α such that the flow rule predicts zero lateral strains for stress states corresponding to Jaky's k_0 values:

$$\alpha = \frac{M(M-9)(M-3)}{9(6-M)} \frac{1}{1-\frac{\kappa}{\lambda_0}} \qquad Eq.\ [35]$$

3.4 State parameters

In addition to the conventional results, it is possible to monitor the evolution of specific model quantities and state variables, as shown in Table 4 (on page 18), useful for plotting the yield surfaces at each step.

Table 4: BBM additional results

User-defined parameters	Symbol	Description	Unit
1	$p_0{}'$	Preconsolidation pressure of fully saturated state	kPa
2	*suction*	Suction	kPa
3	$p_c{}'$	Preconsolidation pressure of unsaturated state	kPa
4	$p_t{}'$	Tensile strength	kPa
5	p_w	Pore water pressure	kPa

User-defined parameters	Symbol	Description	Unit
6	p_{eq}	Equivalent pressure	kPa
7	OCR_{iso}	Ratio of unsaturated preconsolidation pressure over the equivalent pressure	-
8	$Flag_{init}$	Flag indicating that the initialisation has been completed (e.g.123)	-

The equivalent pressure is calculated as:

$$p_{eq} = \frac{3J^2}{\left(\frac{g(\theta)}{g(-1)}\right)^2 M^2\left(p' + p_t'\right)} + p' \qquad Eq.\ [36]$$

4 Simulation of laboratory tests

The PLAXIS BBM model can be used to simulate both unsaturated and fully saturated soils, and, therefore, the transition from an unsaturated to saturated state, and vice versa. Several laboratory tests have been simulated using PLAXIS SoilTest to highlight the model features.

To simulate the unsaturated condition in PLAXIS 2023.1 SoilTest it is necessary to activate ***Suction*** in the ***Options*** menu as shown in Figure 10 (on page 20).

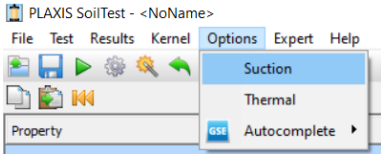

Figure 10: Options menu in SoilTest for activating Suction

In all tests (except from the Pressuremeter test), it is possible to enter an initial suction. The input stresses are required in terms of total stresses. Based on the hydraulic parameters specified for the material to test, the effective saturation S_e is calculated and showed in a non-editable box. This quantity is used to calculate the active pore pressure (Eq. [5]) and, consequently, the effective stresses (also shown in a non-editable box). Figure 11 (on page 20) shows the new SoilTest user-interface in the case of a triaxial test.

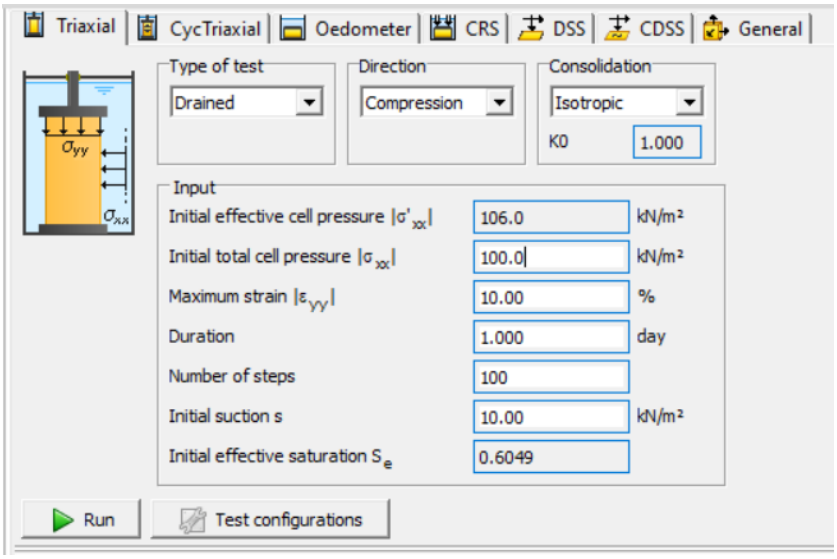

Figure 11: SoilTest window showing Triaxial test input with suction

4.1 Triaxial tests on fully saturated samples

Given the implementation of Lode's angle dependency (based on Sheng et al., 2000 (on page 54)), PLAXIS BBM represents an improvement of the well-known Modified Cam-Clay model (MCC) for a fully saturated state, as shown by the following results of drained triaxial test simulations in compression and extension.

The value of each parameter is given in Table 5 (on page 21) and is valid for both models. The other parameters characterising BBM are not relevant in the case of a fully saturated sample, and they can be set equal to zero.

The tests are performed on normally consolidated (OCR=1) samples, sheared at a confining pressure of 500kPa. This condition is achieved setting the desired OCR value in the case of BBM, while for MCC, the vertical preconsolidation pressure must be defined.

Table 5: Values for BBM and MCC model parameters

Symbol	Description	Value	Unit
ν'	Poisson's ratio	0.3	-
κ	Slope of the swelling line in the (v, $ln\ p'$) plane	0.025	-
λ	Slope of the compression line of the fully saturated material, in the (v, $ln\ p'$) plane	0.10	-
φ	Friction angle at critical state	25.4	o
e_0	Initial void ratio	1	-
p_r	Reference effective pressure	5	kPa
α	Coefficient of the plastic potential	1	-
$k0_{NC}$	Coefficient of earth pressure at rest in normal consolidation	1	-
OCR	Overconsolidation ratio	1	-
POP	Pre-Overburden pressure	0	kPa

Figure 12 (on page 22) summarizes the results of drained triaxial tests. A perfect agreement between BBM and MCC models can be deduced for the triaxial compression case. However, in extension, results show a critical state stress ratio equal to 1, as in compression, for MCC in contrast to 0.75 for BBM. This difference is due to the influence of Lode's angle on the yield for BBM.

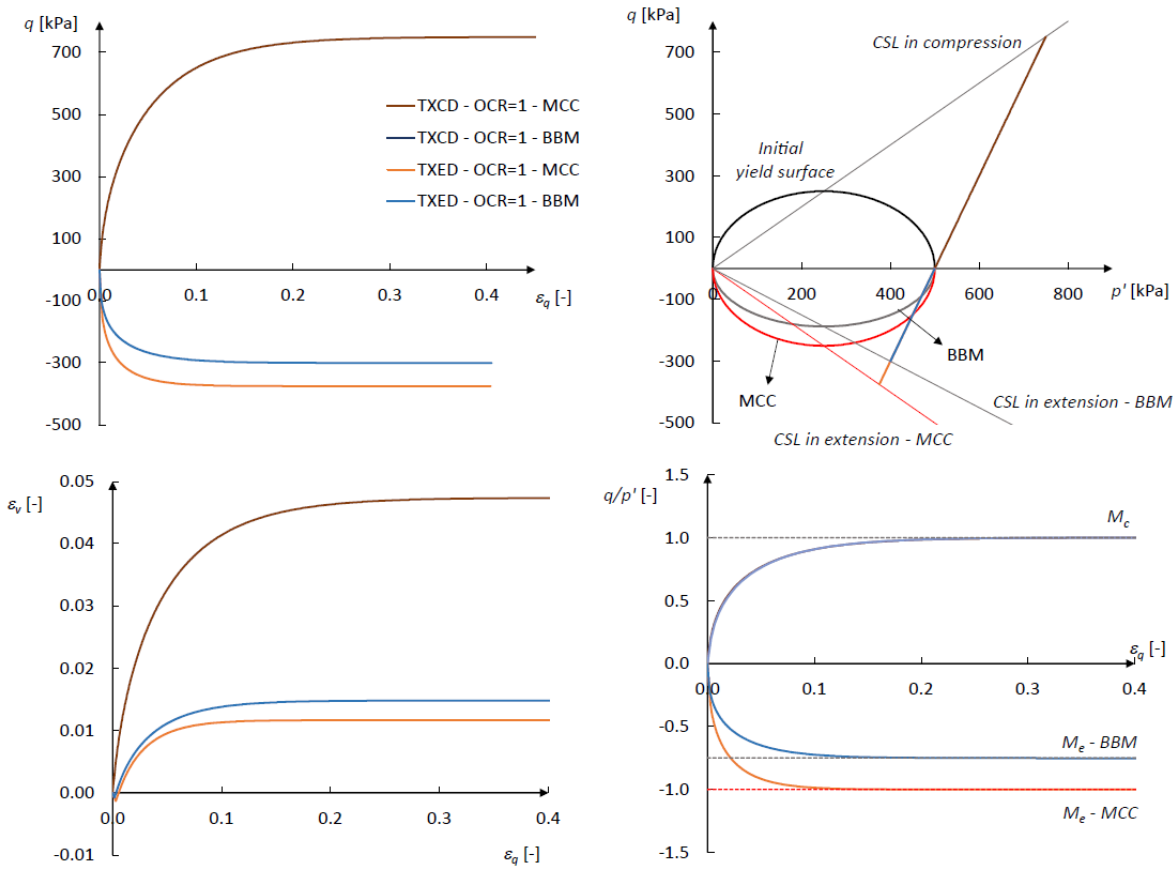

Figure 12: Triaxial drained tests on fully saturated BBM and MCC, in compression and extension

Furthermore, the PLAXIS BBM allows to account for a non-associated flow rule also in the case of full saturation, representing a further extension to the MCC model. The previous results are compared with the case of α equal to 0.474 in Figure 13 (on page 23). Along the same drained triaxial compression stress path, larger volumetric strains are initially generated, but the maximum reached value is the same as in the case of the associated flow rule. In the $(\varepsilon_q,\ q)$ plane, this also results in a stiffer response at low deviatoric strains when α is 0.474.

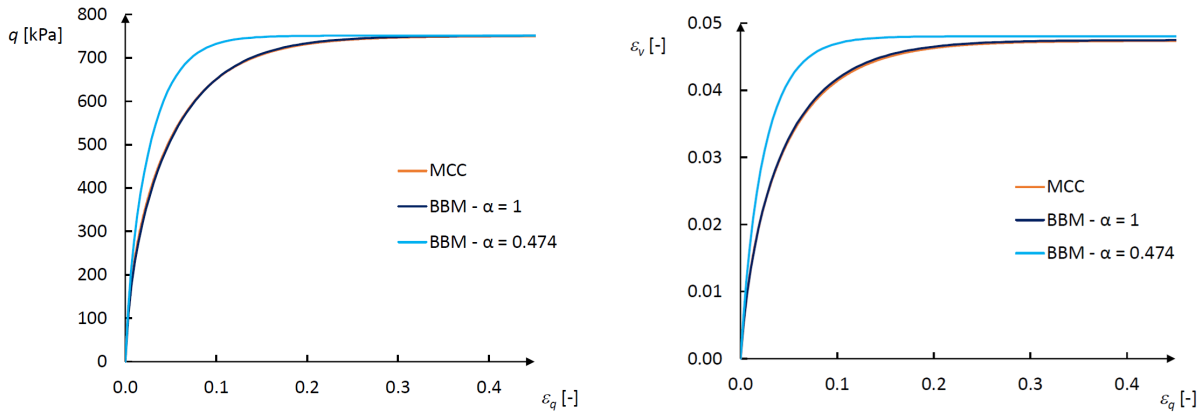

Figure 13: Triaxial compression drained tests on fully saturated BBM with associated (α=1) and non-associated (α=0.474) flow rule, compared with MCC

4.2 Triaxial tests on unsaturated samples

The capabilities of the PLAXIS BBM in simulating the unsaturated behaviour of soils are first shown performing a series of tests characterised by an initial suction s_0. This value is kept constant during drained tests, while it evolves when undrained conditions are considered.

The unsaturated sample is characterised by a certain degree of saturation, used to calculate p_{active} (Eq. [5]) and, therefore, the effective stresses (Eq. [4]), given the initial total stresses. The parameters that control the hydraulic model, given in Table 6 (on page 23), define the SWCC represented in Figure 14 (on page 24).

Table 6: Hydraulic parameters

Symbol	Description	Value	Unit
S_{res}	Residual degree of saturation	0.02427	-
S_{sat}	Degree of saturation in fully saturated conditions	1.0	-
g_a	Fitting parameter related to the air entry value of the soil	0.82	-
g_n	Fitting parameter related to the rate of water extraction	1.218	-
g_c	Fitting parameter equal to $(1 - g_n) / g_n$	-0.17898	-

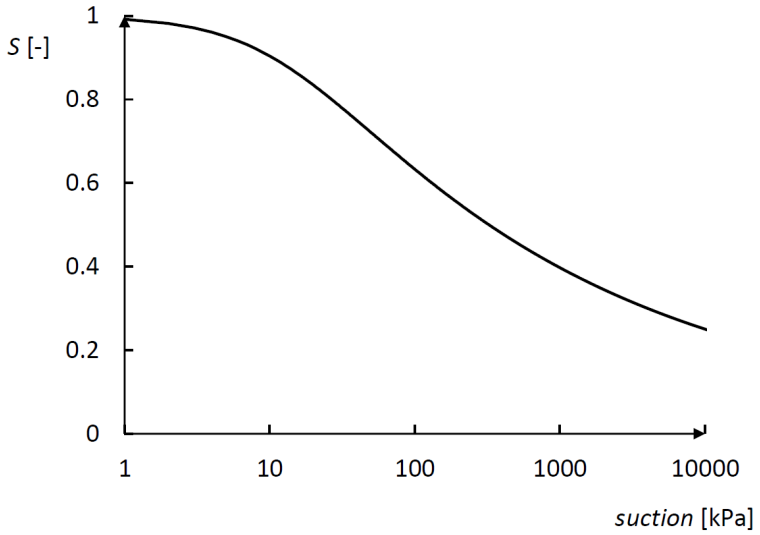

Figure 14: Soil-Water Characteristic Curve based on the hydraulic parameters in Table 6

The same parameter values as in Table 5 (on page 21) are used. In addition, p_r is set equal to 5kPa, r is 0.8 and β is equal to 0.012kPa^{-1}.

Three different values of initial suction are taken into consideration, such as 0, 50 and 100kPa. The initial total mean pressure is isotropic (k_0^{NC} equal to 1) and equal to 100kPa in all cases. The value of OCR is set such that $p_0{}'$ is the same for all cases and equal to 128kPa, also meaning that the LC curve is the same for all samples (Figure 15 (on page 24)). Note that, due to the use of Bishop's effective stresses, the yield functions are defined in terms of effective stresses while the initial stresses and the loading condition are defined in terms of total stresses.

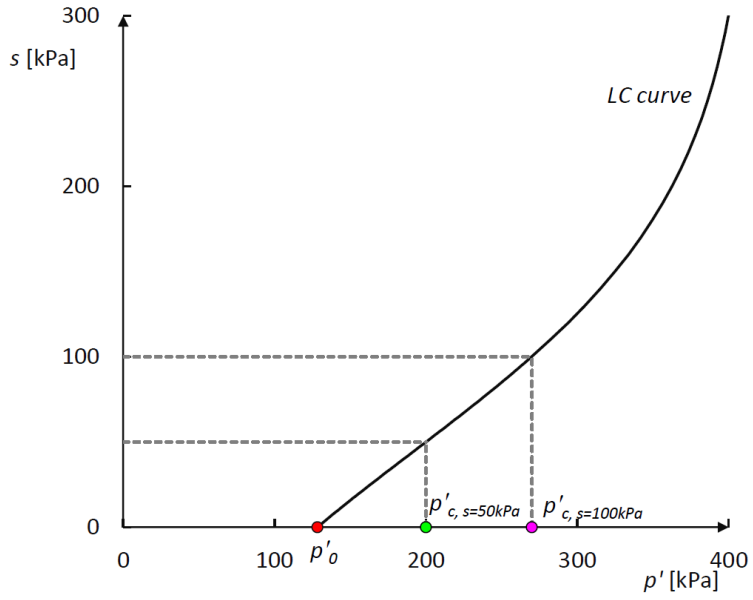

Figure 15: Initial LC curve for parameters in Table 5 and p_r= 5 kPa, r = 0.8 and β = 0.012 kPa^{-1}

As for the contribution to cohesion given by the parameter k_s, triaxial tests have been simulated considering its value equal to 0 and 0.3. The yield surfaces for different values of suction, and considering k_s equal to 0 and 0.3, are shown in Figure 16 (on page 25).

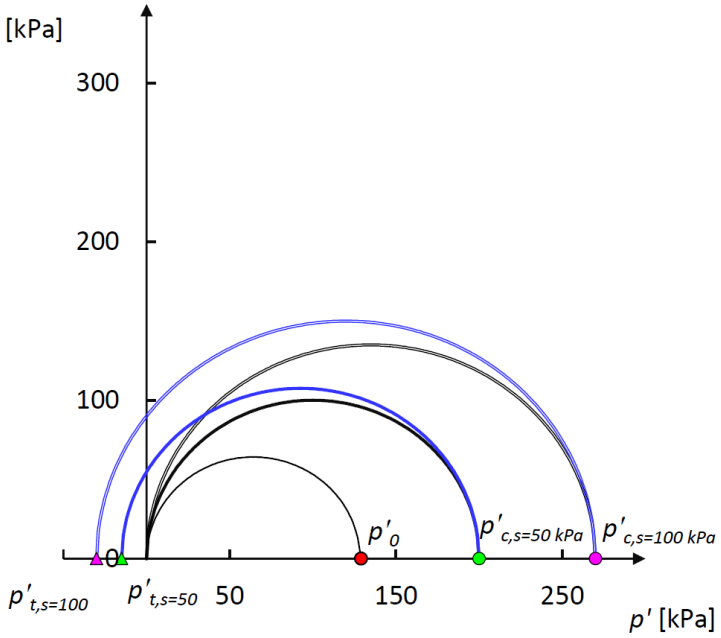

Figure 16: Initial yield surfaces for different values of suction, considering k_s equal to 0 and 0.3

Table 7 (on page 25) summarises the value of S_{eff}, p_{active}, $p_c{}'$, $p_t{}'$ and λ_s for each initial value of suction. When k_s is 0, $p_t{}'$ is equal to zero in all cases .

Table 7: Initial state for each value of initial suction. (*) for k_s = 0.3

Suction [kPa]	S_{eff} [-]	p_{active}[kPa]	p [kPa]	p' [kPa]	OCR [-]	p'_c [kPa]	p'_t (*) [kPa]	λ_s [-]
0	1	0	100	100	1.280	128	0	0.10
50	0.7138	35.69	100	135.69	1.474	200	-15	0.0909
100	0.6237	62.37	100	162.37	1.663	270	-30	0.0860

4.2.1 Drained triaxial compression tests

Triaxial drained compression tests at constant suction are simulated, starting from a total mean pressure of 100kPa and up to an axial strain of 30% to ensure that a critical state condition is reached. Since all samples are

characterised by an OCR larger than one, the simulated response is purely elastic until the current effective stress touches the corresponding yield surface.

4.2.1.1 No contribution of suction to cohesion$(k_s = 0)$

The first set of tests is performed considering no contribution of suction to cohesion (k_s equal to 0). An increase in suction causes an increase in deviatoric stress (Figure 17 (on page 26)), while the volumetric strains are lower for higher suction values, also due to the different OCR associated to each sample, given the same initial total mean pressure. Since k_s is zero, the stress ratio at critical state is the same for all values of suction, and it is equal to 1.

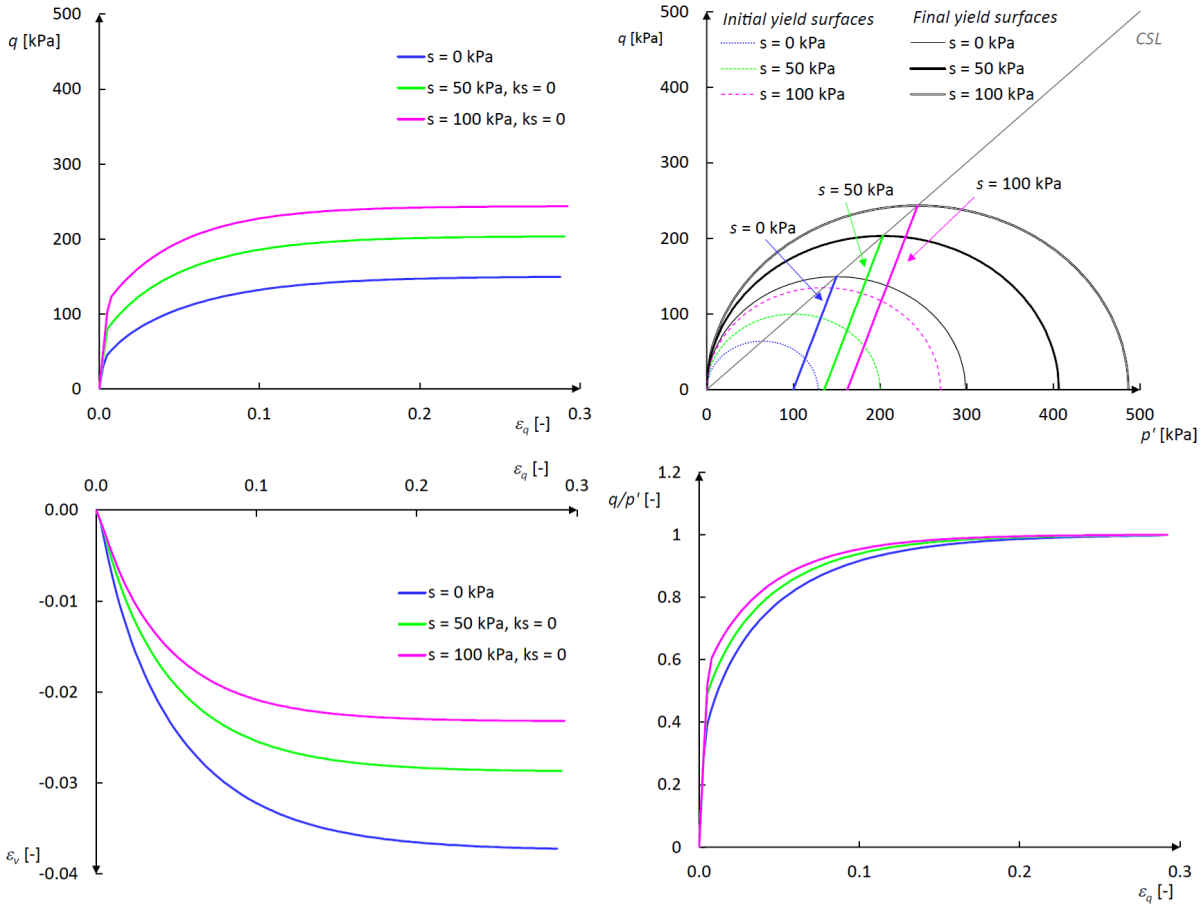

Figure 17: Results of TXCD tests at different constant suction values, with $k_s = 0$

The evolution of the yield curve in the (p', s) plane (i.e., the LC curve) for each sample is shown in Figure 18 (on page 27).

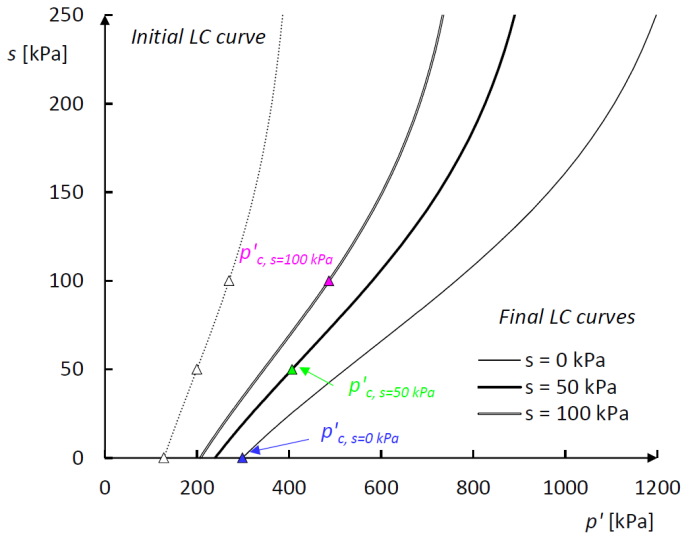

Figure 18: LC curves at the beginning and end of the triaxial compression tests, with k_s = 0

4.2.1.2 Contribution of suction to cohesion (k_s = 0.3)

The same tests have been simulated setting k_s equal to 0.3. The results are shown in Figure 19 (on page 28). At the same constant suction, the maximum deviatoric stress is consistently larger with respect to the previous case, where no contribution of suction to cohesion is considered (dashed curves in Figure 19 (on page 28)). The volumetric strains follow the same trend as in the case of k_s equal to zero, but, for the same suction value, they are larger when some cohesion is considered. Even considering a constant value of M (equal to 1) in all cases, the stress ratio at critical state is larger for increasing suction due to the tensile strength, which shifts the yield surface towards the negative side of the p' axis.

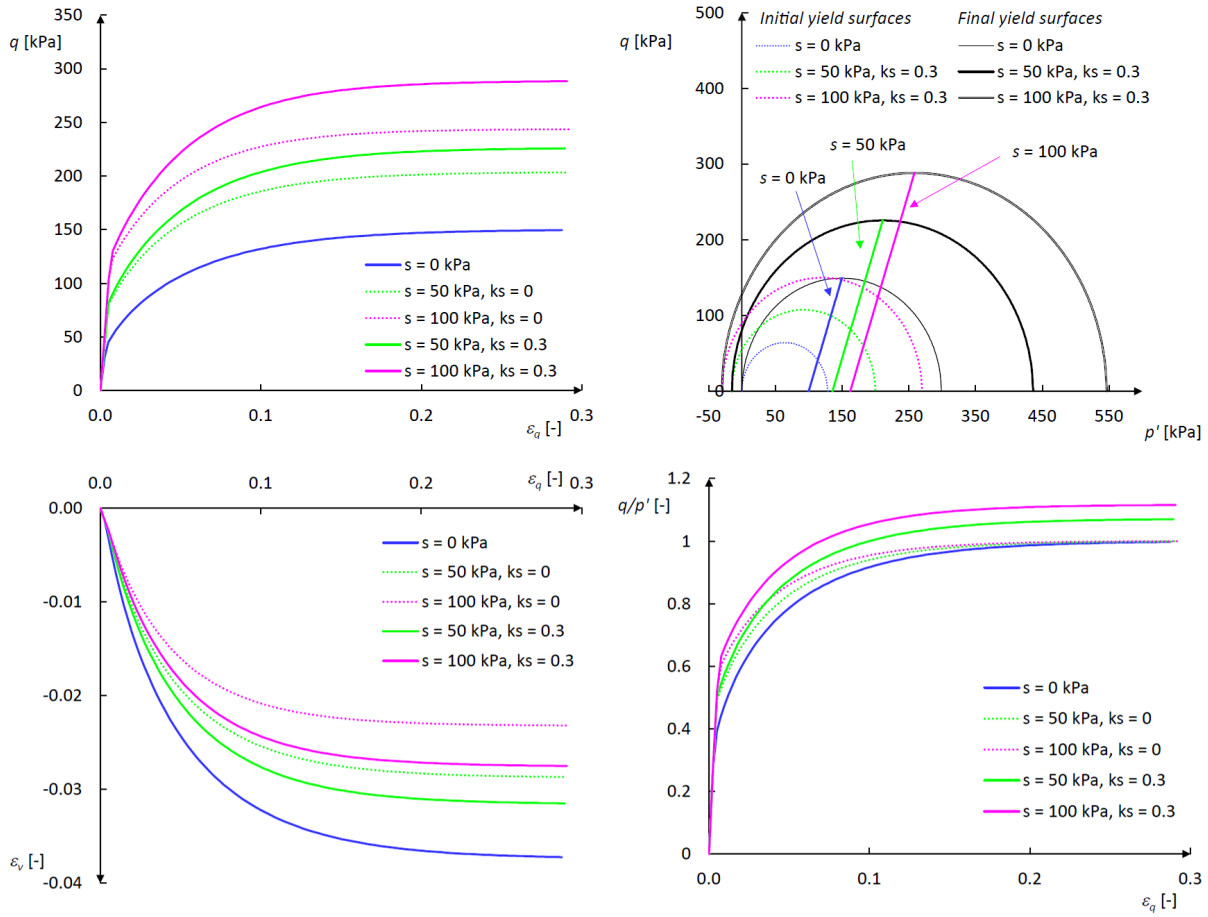

Figure 19: Results of TXCD tests at different constant suction values, with k_s = 0.3, compared to the case of k_s = 0

The evolution of the LC curves is shown in Figure 20 (on page 29).

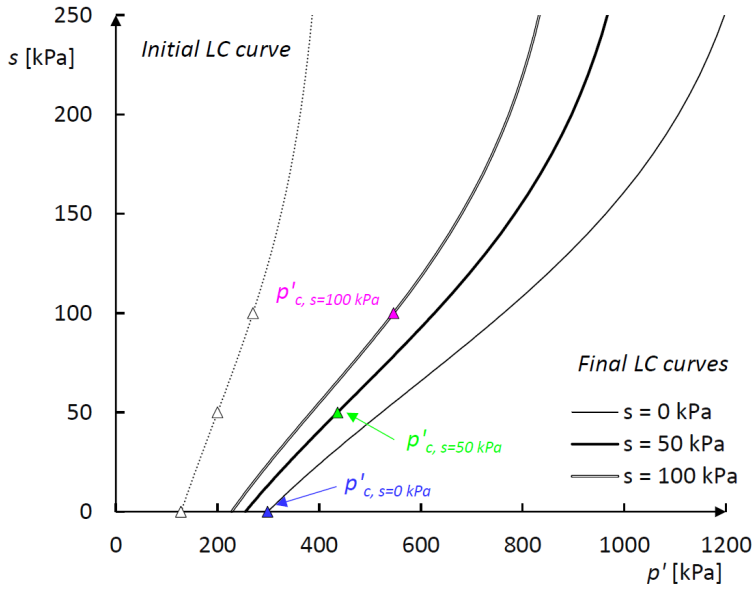

Figure 20: LC curves at the beginning and end of the triaxial compression tests, with k_s = 0.3

4.2.2 Undrained triaxial compression tests

The same tests performed in section Contribution of suction to cohesion (ks = 0.3) (on page 28) with k_s equal to 0.3 are performed in undrained conditions as shown in Figure 21 (on page 30). When suction is zero, no volumetric strains can develop, and excess pore pressures are generated. Instead, when suction is not zero, both excess pore pressures and volumetric strains develop and suction (and saturation) in the sample changes during the test as shown in Figure 22 (on page 30), which also means that $p_t{}'$ evolves during the test.

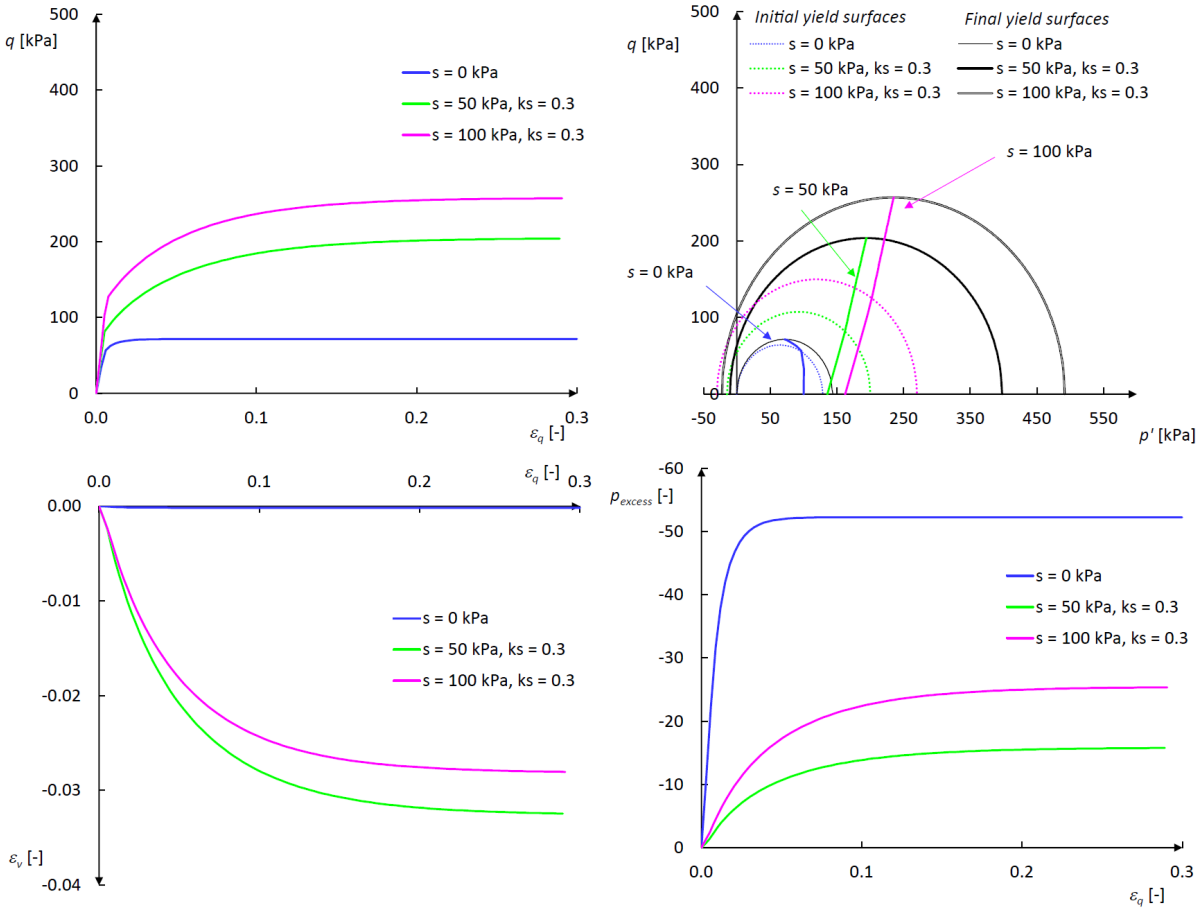

Figure 21: Results of TXCU tests at different initial suction values, with k_s = 0.3

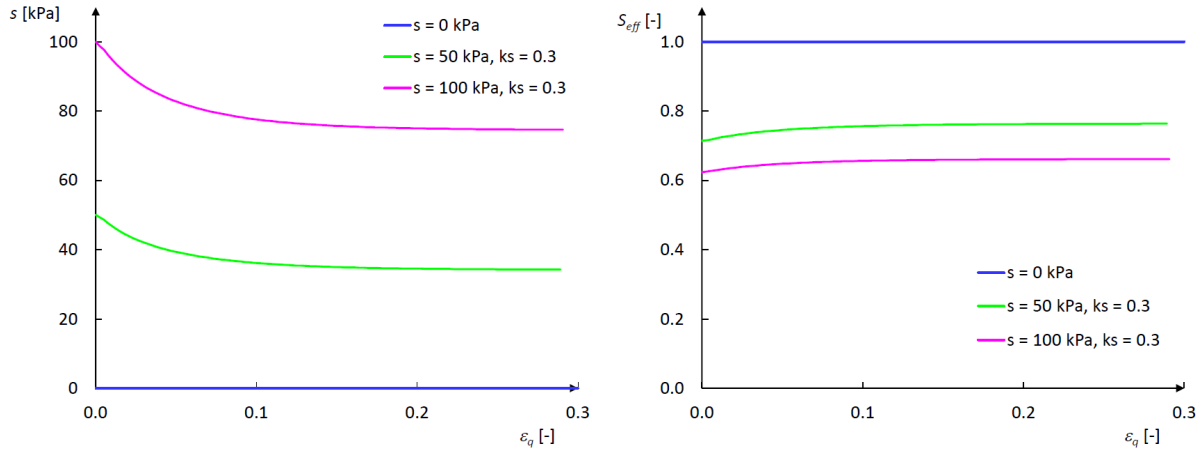

Figure 22: Variation of suction and effective saturation during TXCU tests, starting from different initial suction values and with k_s = 0.3

At the end of each TXCU test, the LC curve has evolved differently depending on the initial value of suction, as shown in Figure 23 (on page 31).

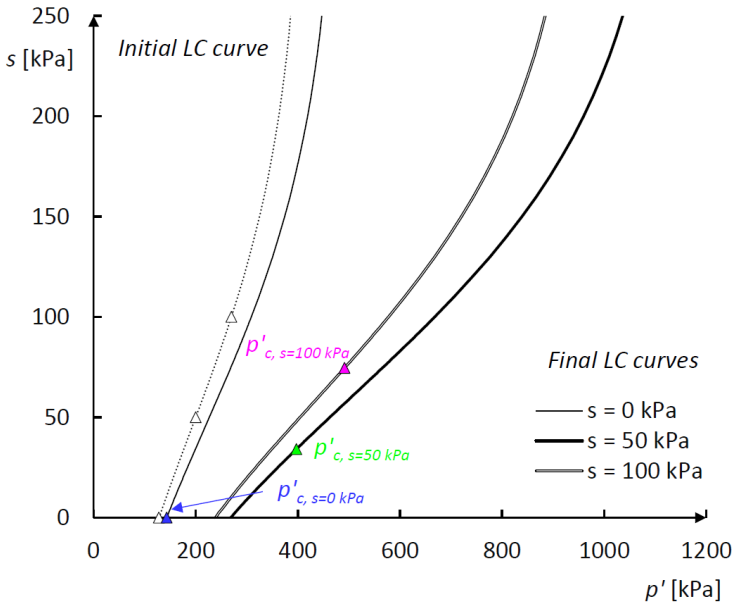

Figure 23: Evolution of the LC curve at the end of each TXCU test for different values of initial suction

4.3 Laboratory test with drying-wetting path

The simulation of laboratory tests consisting of multiple phases during which suction is increased (drying) or decreased (wetting) allows to show the model capabilities of reproducing both elastic swelling and plastic collapse due to wetting, as well as other distinctive features of the behaviour of unsaturated soils (described in paragraph The unsaturated soil behaviour (on page 4)).

This test consists of four phases during which changes in suction at constant total pressure, as well as a change in total pressures at constant suction, are simulated. The prescribed suction and total mean pressure during the four phases are shown in Figure 24 (on page 32).

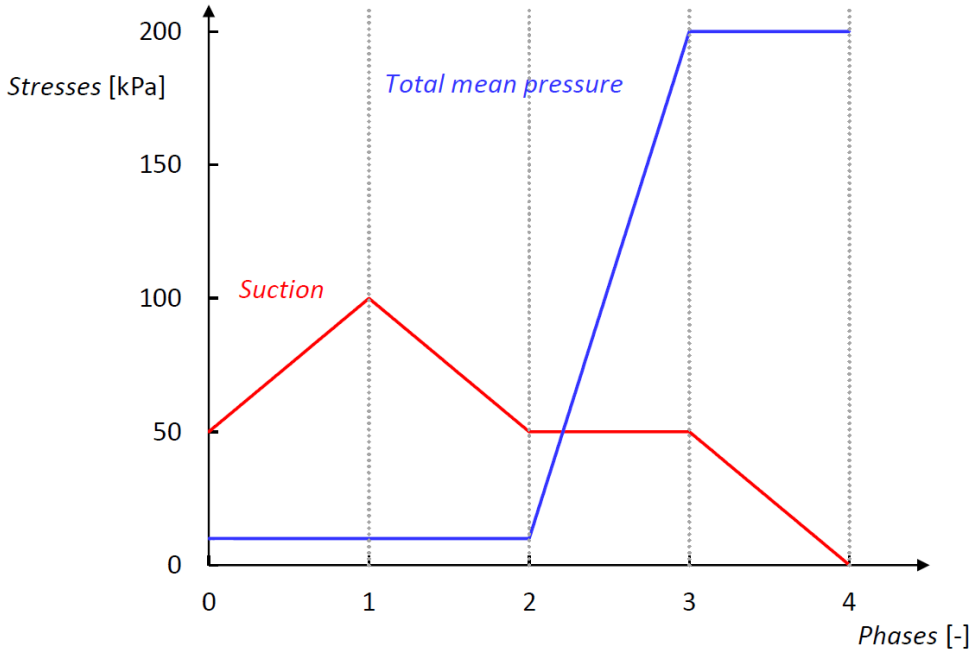

Figure 24: Value of suction and total mean pressure in each of the four test phases

At the initial state, the total stress state is isotropic and equal to 10kPa, and the initial suction is 50kPa. The sample is overconsolidated (OCR = 4.4) and the effective saturation is 71.38%, meaning that the initial effective mean pressure is equal to 45.7kPa. This results in an initial value of p_c' equal to about 200kPa and a value of p_0' equal to about 128kPa. Therefore, the initial yield surface is the same as the one previously shown for the triaxial tests at the same suction as shown in Figure 25 (on page 32).

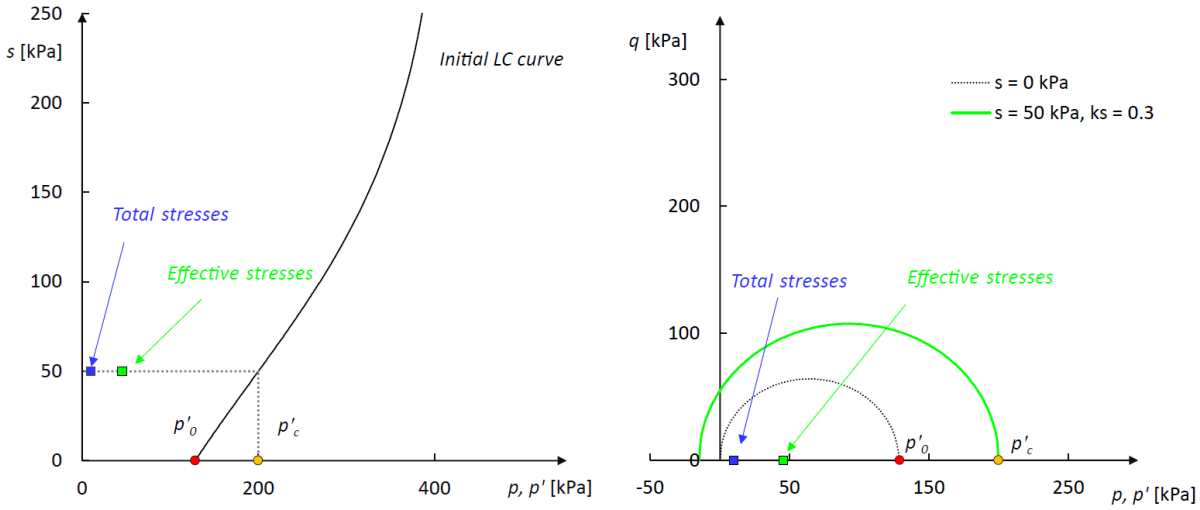

Figure 25: Initial yield surface plotted in the stress planes, together with the initial stress state

A summary of the model parameters is shown in Table 8 (on page 33). The values are the same as the ones used in the triaxial undrained tests (paragraph Undrained triaxial compression tests (on page 29)) with the additional value of 0.01 for the slope of the swelling line due to an elastic suction variation, κ_s, and an OCR equal to 4.4.

Table 8: BBM model parameters for the simulation of the drying-wetting path

Symbol	Description	Value	Unit
ν'	Poisson's ratio	0.3	-
κ	Slope of the swelling line in the (v, $ln\ p'$) plane	0.025	-
λ	Slope of the compression line of the fully saturated material, in the (v, $ln\ p'$) plane	0.10	-
κ_s	Slope of the swelling line in the (v, $ln\ s$) plane	0.01	-
k_s	Factor accounting for tensile strength due to suction	0.3	-
φ	Friction angle at critical state	25.4	o
e_0	Initial void ratio	1	-
p_r	Reference mean effective pressure	5	kPa
r	Parameter controlling the soil stiffness with suction	0.8	-
β	Parameter controlling the rate of increase of soil stiffness with suction	0.012	kPa^{-1}
α	Coefficient of the plastic potential	1	-
$k0_{NC}$	Coefficient of earth pressure at rest in normal consolidation	1	-
OCR	Overconsolidation ratio	4.4	-
POP	Pre-Overburden pressure	0	kPa

4.3.1 Phase 1: Drying

The first phase consists of an elastic increase of suction to 100kPa, at constant total stress, while the effective mean pressure increases from about 45 to about 72kPa. The LC curve does not change but the elastic domain increases due to the higher suction as shown in Figure 26 (on page 34).

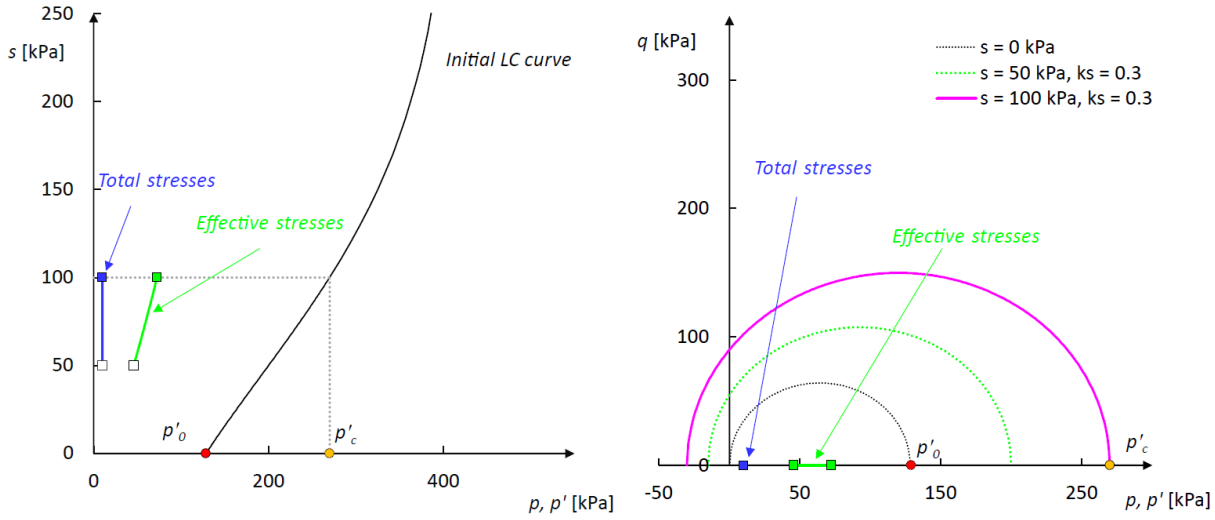

Figure 26: Drying path and evolution of the yield surface in the (p', q) plane (Phase 1)

Drying induces contraction of the sample and the slope of the drying path in the ($ln\ p'$, s) plane is a function of both κ_s and κ as shown in Figure 27 (on page 34).

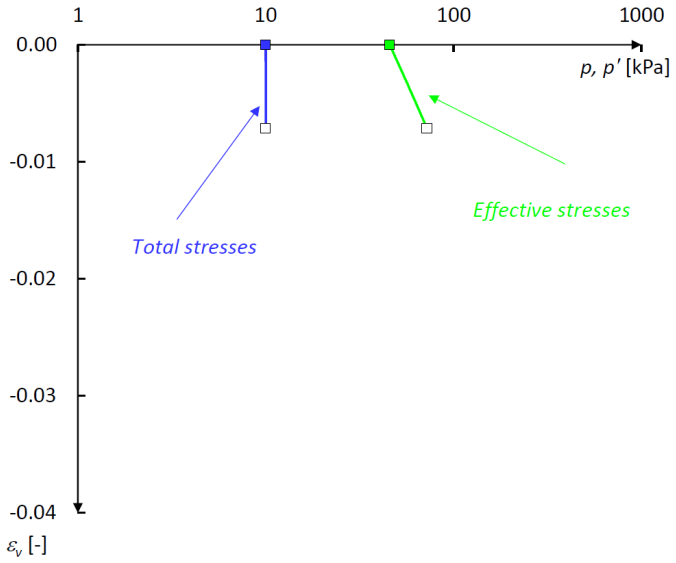

Figure 27: Elastic contraction due to drying (Phase 1)

4.3.2 Phase 2: Wetting

The second phase consists in wetting the sample at the same constant total pressure of 10kPa, to a suction of 50kPa. This phase as shown in Figure 28 (on page 35) is fully elastic and brings the yield surface in the same configuration as in the beginning.

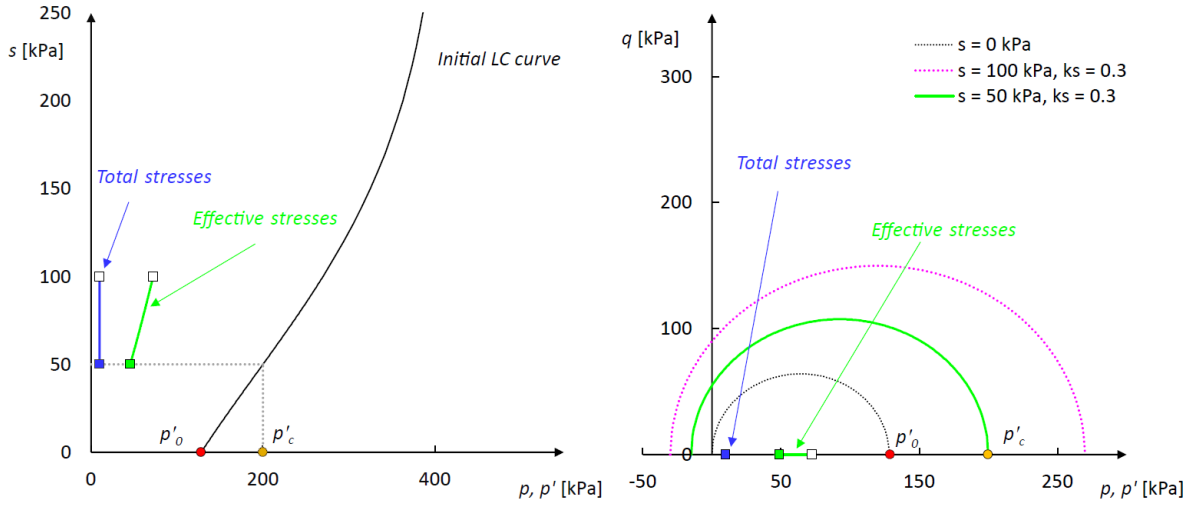

Figure 28: Wetting path and evolution of the yield surface in the (p', q) plane (Phase 2)

The elastic swelling is again a function of both κ_s and κ since any change in suction is always accompanied by a change in effective stresses as shown in Figure 29 (on page 35).

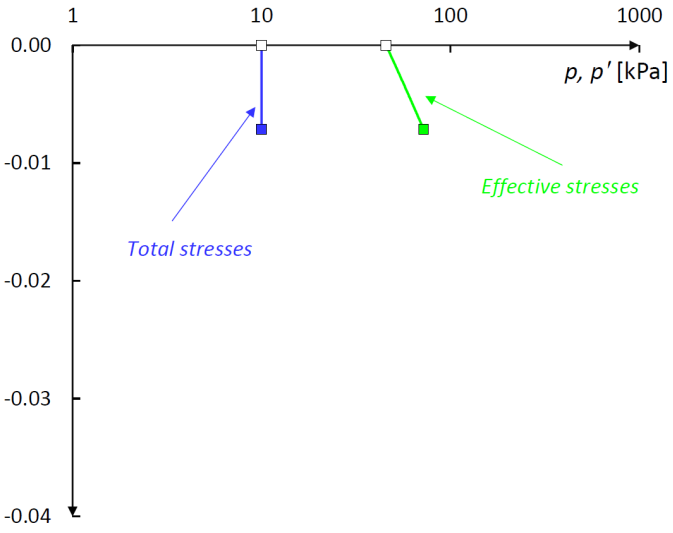

Figure 29: Elastic swelling due to wetting (Phase 2)

4.3.3 Phase 3: Total stress loading

During the third phase, the sample is loaded in drained conditions at a constant suction of 50kPa. The applied total stress increment is isotropic and equal to 190kPa . Therefore, the total mean pressure increases from 10 to 200kPa. In terms of effective mean pressure, the value increases up to 236kPa. In Figure 30 (on page 36), the stress paths show that the model response is initially elastic (up to a total mean pressure of about 163kPa) and then it becomes plastic. Due to positive plastic volumetric strains and to the hardening rule characterising the constitutive model (Eq. [24]), an increase in p_0' and, consequently, in p_c' can be observed.

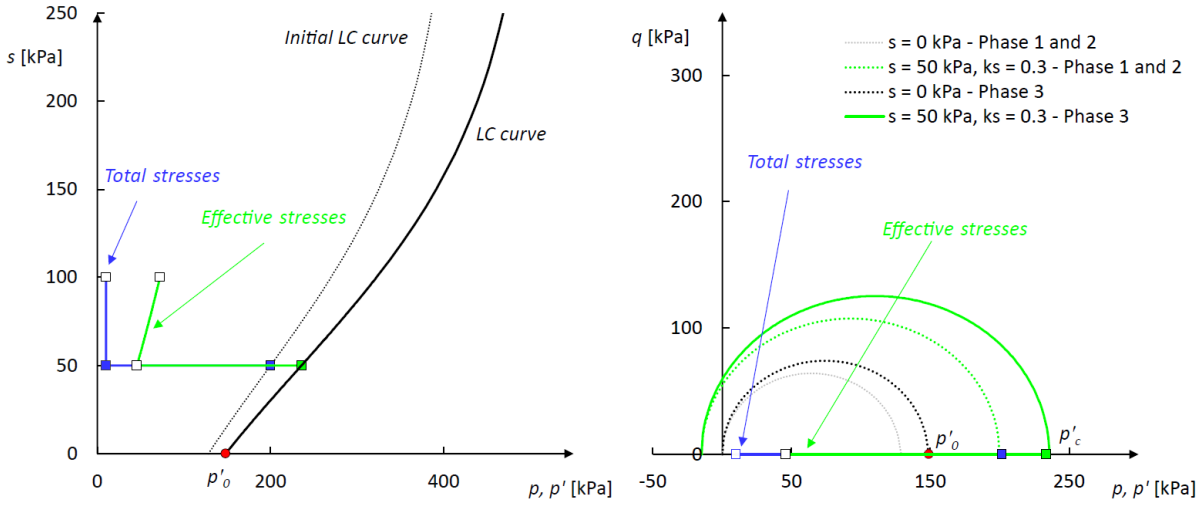

Figure 30: Evolution of the yield surface in the stress planes (Phase 3)

The volumetric response is shown in Figure 31 (on page 37). Up to the initial preconsolidation pressure $p_{c,0}'$, elastic contraction is predicted and the slope of the compression line in the $(ln\ p', \varepsilon_v)$ plane is equal to κ^* (i.e., 0.0125 as given by Eq. [31]) since there is no change in suction. The second portion of the compression line has a different slope due to plastic strains and it is equal to λ_s^*. The value of λ_s can be calculated based on Eq. [22] and it is equal to 0.090. Therefore, the modified compression index λ_s^* for suction equal to 50kPa, is obtained dividing λ_s by the specific volume and it is equal to 0.045.

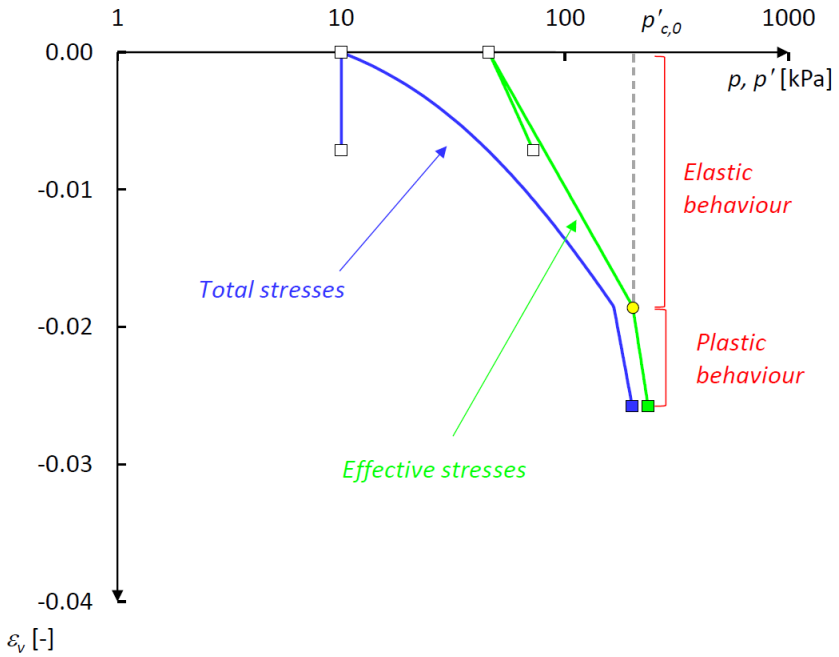

Figure 31: Elasto-plastic isotropic compression (Phase 3)

4.3.4 Phase 4: Wetting

The final phase consists in wetting the soil sample to complete saturation, at constant total mean pressure. The reduction of suction from 50 to 0kPa also means a decrease in effective stresses from 236 to 200kPa. The evolution of the yield surface in the stress planes is shown in Figure 32 (on page 38). The yield surface in the (p', q) plane converges towards the one at full saturation and the total and the effective mean pressures become identical.

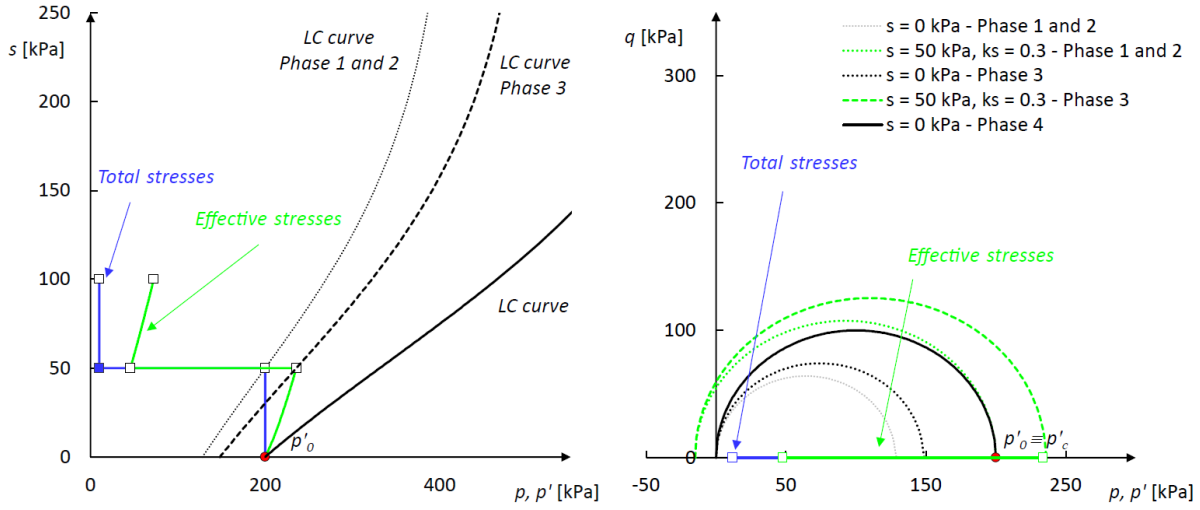

Figure 32: Evolution of the yield surface in the stress planes (Phase 4)

Unlike Phase 2, wetting is here causing a (plastic) irreversible collapse, instead of an elastic swelling. The constitutive model can reproduce this behaviour as it can be observed in Figure 33 (on page 38).

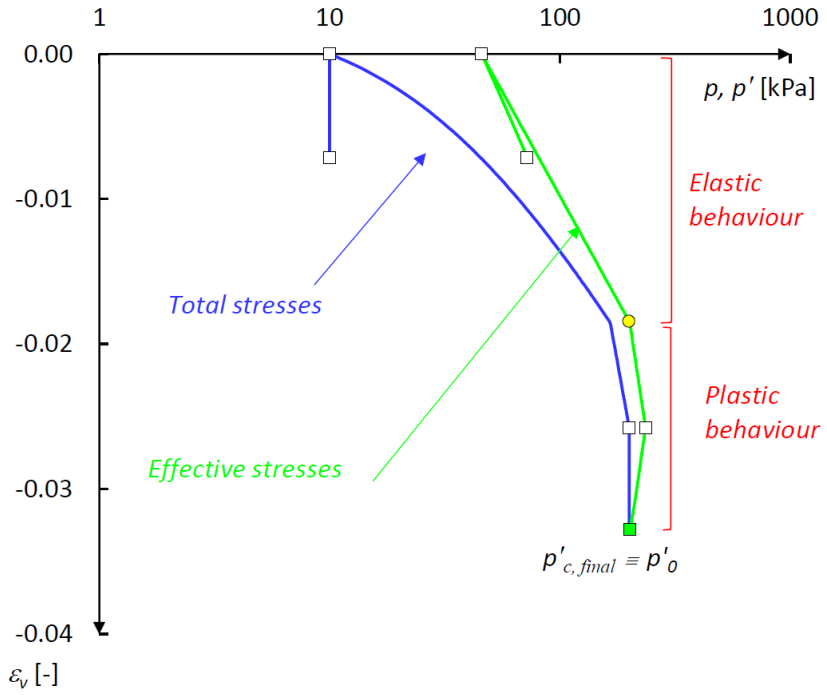

Figure 33: Plastic collapse due to wetting (Phase 4)

5 Finite element analyses with PLAXIS 2D

The performance of the model is further tested in an application to a boundary value problem in PLAXIS 2D.

The application consists in evaluating the settlement of a foundation 2m wide, lying on a homogeneous soil deposit of 8m depth with a water table at 4m depth from the ground surface. Under the soil layer there is a stiff bedrock which is not explicitly modelled. Instead, its effect is described via a mechanically fixed and closed water flow boundary at the bottom of the model.

Due to the symmetry, only half of the physical domain is described in the finite element model (Figure 34 (on page 42)).

The PLAXIS BBM model parameters used for the soil deposit are summarised in Table 9 (on page 39). Note that the interface properties should be explicitly defined even though they are not required in the computation procedure of this project.

Table 9: PLAXIS BBM model parameters for the FEM analysis

Symbol	Description	Value	Unit
General			
Drainage type	-	Drained	-
γ_{unsat}	Unsaturated unit weight	18	kN/m^3
γ_{sat}	Saturated unit weight	20	kN/m^3
e_{init}	Initial void index	1	-
n_{init}	Porosity	0.5	-
Mechanical			
ν'	Poisson's ratio	0.3	-
κ	Slope of the swelling line in the (v, $ln\ p'$) plane	0.015	-

Mechanical			
λ	Slope of the compression line of the fully saturated material, in the ($v,\ ln\ p'$) plane	0.10	-
κ_s	Slope of the swelling line in the ($v,\ ln\ s$) plane	0.005	-
k_s	Factor accounting for tensile strength due to suction	0.8	-
φ	Friction angle at critical state	25.4	o
e_0	Initial void ratio	1	-
p_r	Reference effective pressure	5	kPa
r	Parameter controlling the soil stiffness with suction	0.7	-
β	Parameter controlling the rate of increase of soil stiffness with suction	0.03	kPa^{-1}
α	Coefficient of the plastic potential	0.4183	-
$k0_{NC}$	Coefficient of earth pressure at rest in normal consolidation	0.7291	-
OCR	Overconsolidation ratio	1.1	-
POP	Pre-Overburden pressure	0	kPa

Groundwater			
Classification type	Classification type	USDA	-
SWCC fitting method	Soil Water Characteristic Curve fitting method	Van Genuchten	-
Soil class (USDA)	Soil class (USDA)	Silty clay loam	-

Groundwater			
<2µm	Percentage passing sieve size < 2µm	34	%
2µm-50µm	Percentage passing sieve size between 2µm and 50µm	55	%
Use defaults	Use default permeabilities	Yes	-
Defaults method	Defaults method	From data set	-
k_x	Horizontal permeability	0.1676	m/day
k_y	Vertical permeability	0.1676	m/day
c_k	Change in permeability	1e15	-
$-\psi_{unsat}$	Maximum pressure head	1e4	m

Interfaces			
Stiffness determination	Method for stiffness determination	From E_{oed}	-
E_{oed}^{ref}	Tangent stiffness for primary oedometer loading	1000	kN/m^2
UD-Power	Rate of stress dependency of the interface stiffness	0	-
UD-p^{ref}	Reference stress level	100	kN/m^2
$c_{ref,\ inter}$	Interface cohesion	1	kN/m^2
φ_{inter}	Interface friction angle	25.4	o
ψ_{inter}	Interface dilatancy angle	0	o

Initial			
K_0 determination	Determination of the coefficient of earth pressure at rest	Manual	-
$K_{0,x}$	0.7291	0.7291	-

Initial			
$K_{0,x} = K_{0,z}$	Use same value of K_0 in both horizontal directions	Yes	-

The geometric characteristics of the problem (Figure 34 (on page 42)) are the following:

- Plane strain with 6-noded elements to reduce the calculation time
- Width 10m and depth 8m
- Line load to simulate the foundation, with a uniformly distributed value of 50kN/m/m in the vertical direction.

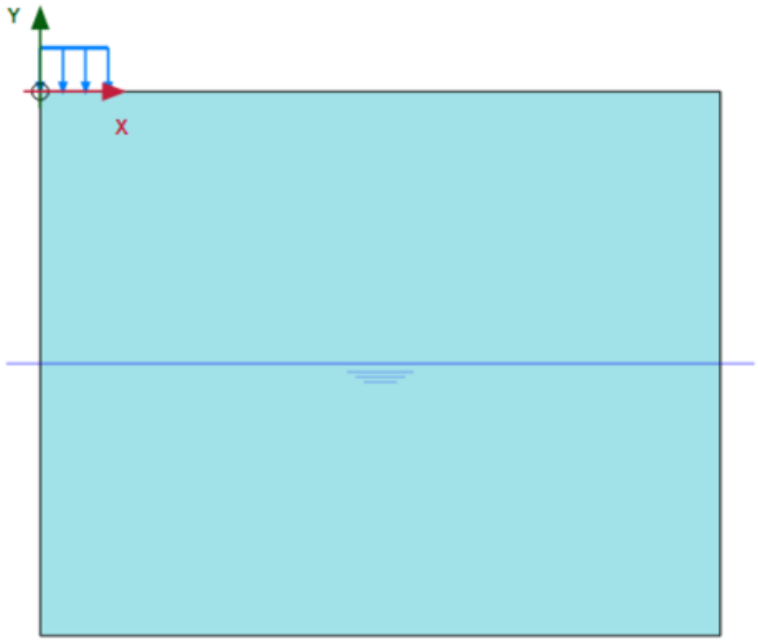

Figure 34: Geometry of the simulated boundary value problem in 2D

Five calculation phases are considered:

1. An initial phase where the stresses are initialised using a K0-procedure.
2. A plastic nil-phase that can be used to inspect the value of the PLAXIS BBM state parameters (paragraph State parameters (on page 18)).
3. A plastic phase for the foundation installation (i.e., the activation of the load).
4. A phase in which a fully coupled flow-deformation analysis is performed to simulate the water table rising from -4m to -2m in 30 days and kept constant for other 30 days.
5. A phase (also performed after the foundation installation) in which a fully coupled flow-deformation analysis is performed to simulate a precipitation event with an infiltration of 0.01 m^3/day for 30 days and that stops after 2 days (Figure 35 (on page 43)).

The last two phases simulate two wetting scenarios corresponding to a phreatic level raise and a rainfall event .

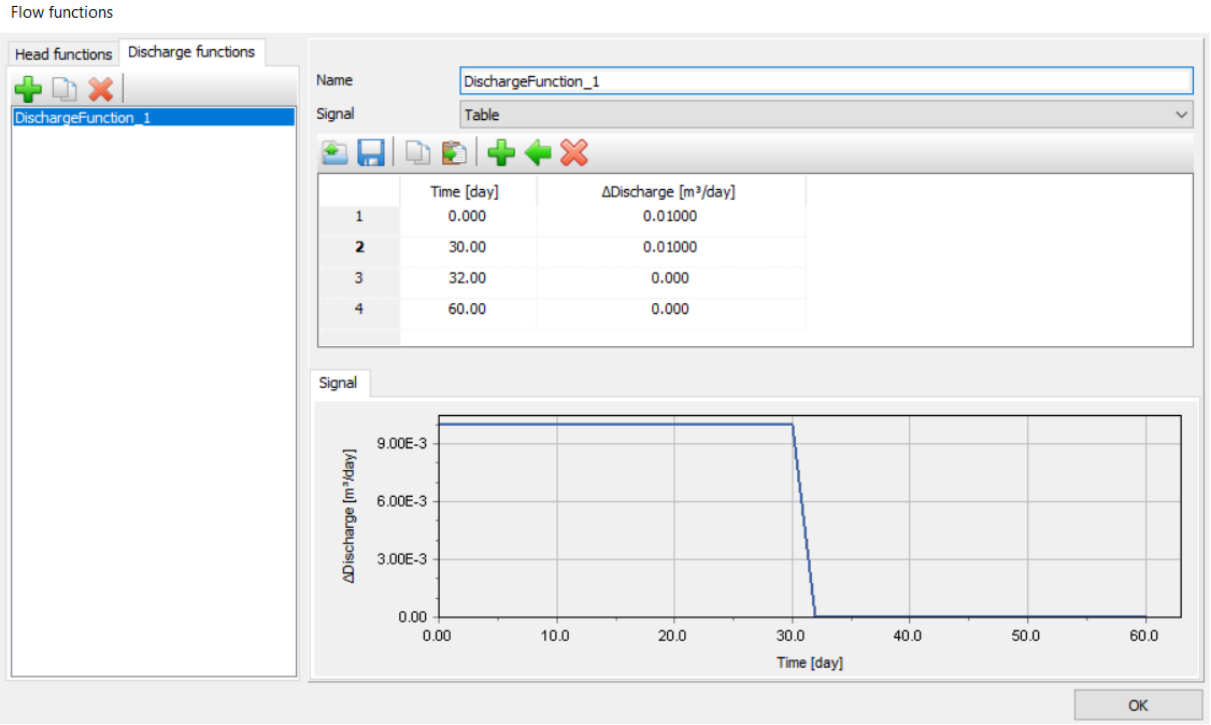

Figure 35: Discharge function

The left and bottom groundwater flow boundaries are closed, as well as the portion at the top where the foundation is installed.

Three nodes and stress points have been selected at:

- x = 0 m, y = 0 m (Node A, Stress point N);
- x = 0 m, y = -2 m (Node B, Stress point O);
- x = 3 m, y = 0 m (Node C, Stress point P).

Given the phreatic level at a depth of 4m from the surface, suction linearly increases from 0 (at -4m) to 40kPa at the ground level, at the initial state of the model in Phase 1 (Figure 36 (on page 44)). Therefore, the vertical effective stresses do not start from 0 but from a value equal to $-p_{active}$, i.e., $-\left(suction \times S_{eff}\right) = 40kPa \times 70.45\ \% = -28.19kPa$ (Figure 37 (on page 44)).

The PLAXIS BBM is initialised such that, below the water table, $p_0{}'$ coincides with $p_c{}'$ (full saturation), while above the water table, $p_c{}'$ increases with increasing suction being also a function of the current stresses (Figure 38 (on page 45)). Similarly, $p_t{}'$ linearly increases with increasing suction due to the factor k_s equal to 0.8 (Figure 39 (on page 45)). The deposit is slightly overconsolidated (OCR=1.1), so the initial stress state is elastic everywhere.

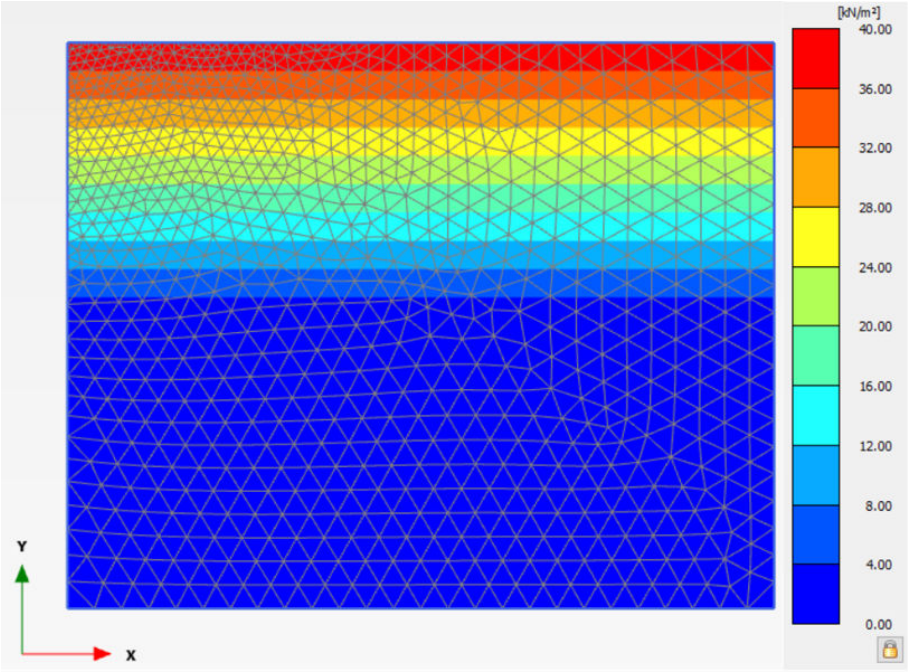

Figure 36: Suction distribution at the beginning (Phase 1)

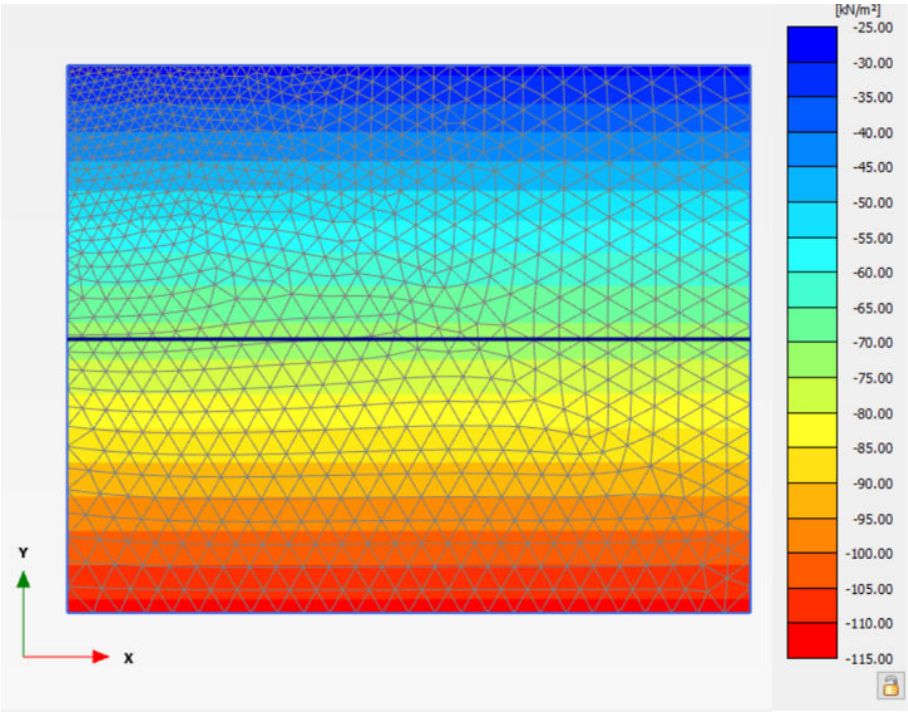

Figure 37: Vertical effective stress distribution at the beginning (Phase 1)

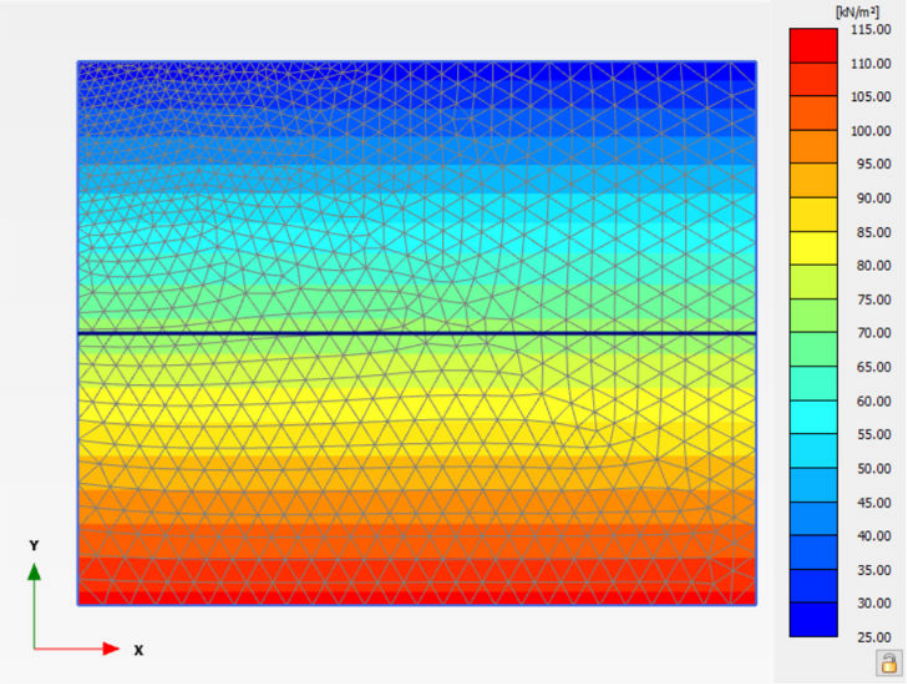

Figure 38: Value of $p_c{}'$ at the beginning (Phase 1)

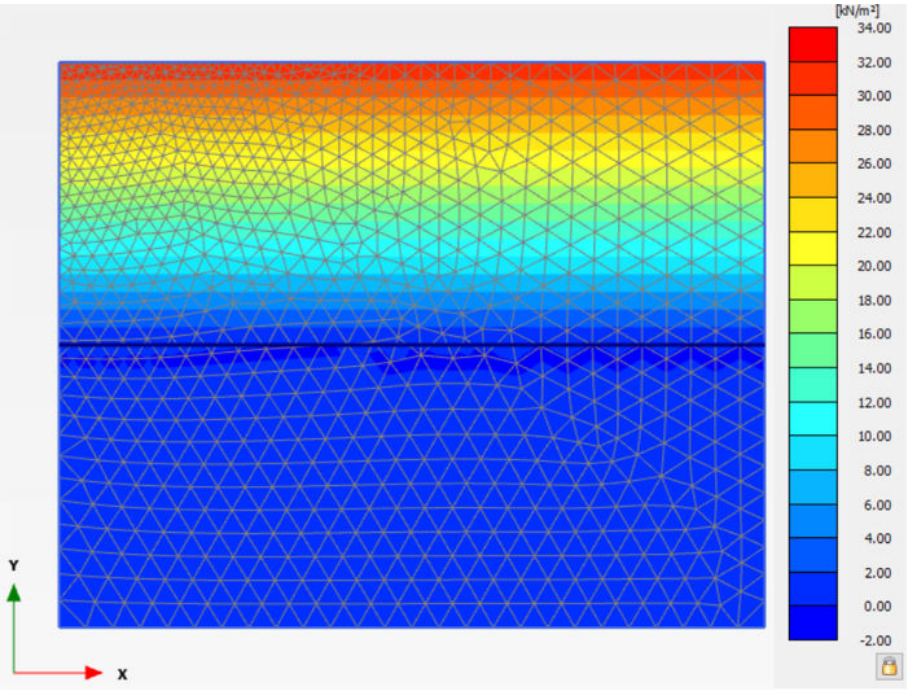

Figure 39: Value of $p_t{}'$ at the beginning (Phase 1)

After the (long term, assumed drained) foundation installation, the distribution of suction remained unchanged, and so the contribution of suction to tensile strength p_t'. On the other hand, stress distribution is modified under the effect of the line load from the foundation, causing an evolution of the yield surfaces in every point, as seen in Figure 40 (on page 46), relative to p_c'.

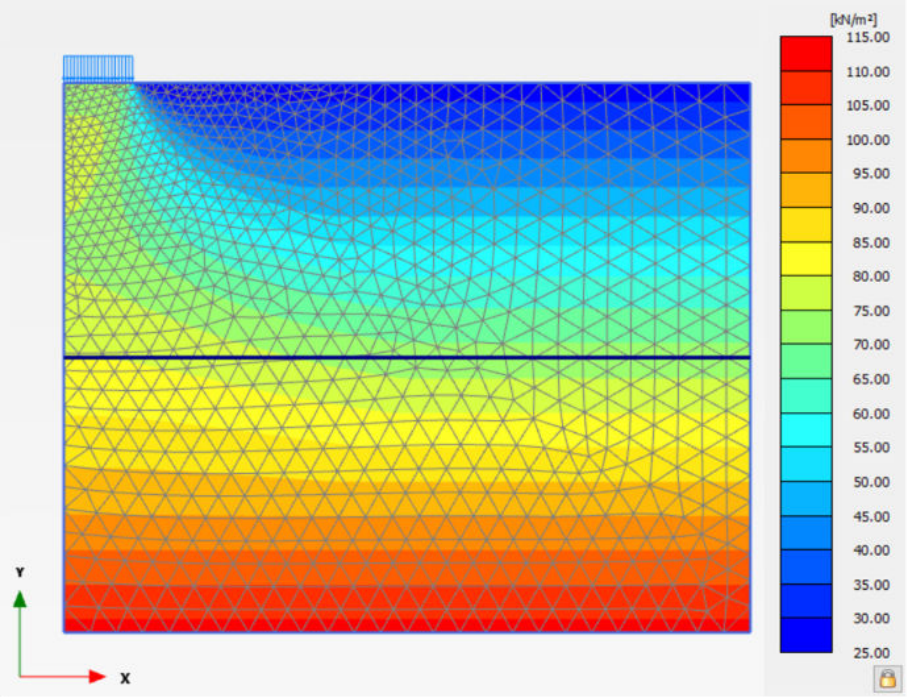

Figure 40: Value of p_c' at the end of the foundation installation (Phase 2)

Figure 41 (on page 47) shows that the behaviour is initially elastic in all selected points (p_0' is constant) but, due to the load application, the behaviour becomes plastic below the foundation (stress points N and O) (p_0' and p_c' increase), while in Stress point P, the behaviour remains elastic. Since there is no change in suction, p_t' is constant throughout Phase 2.

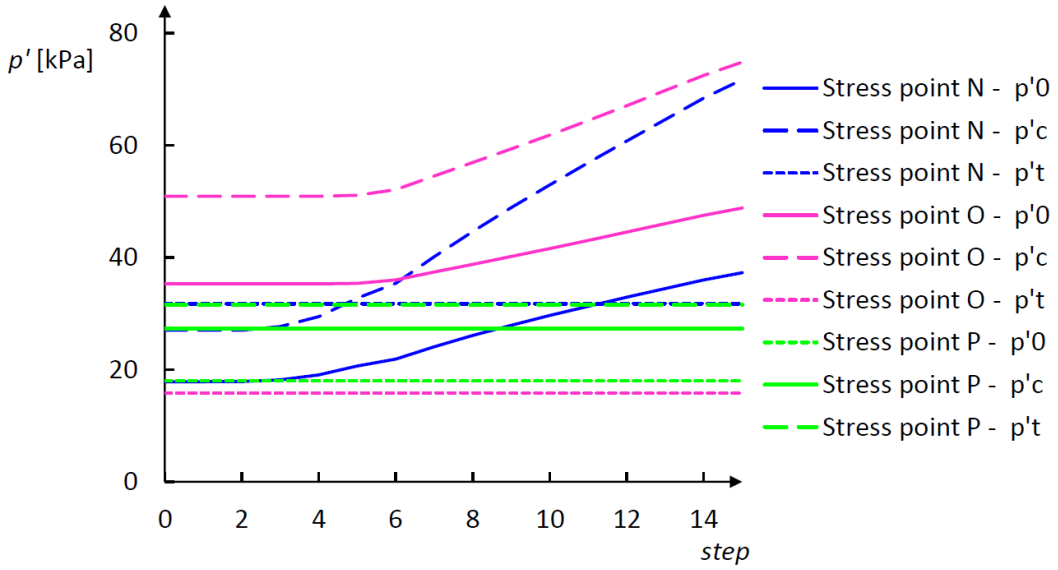

Figure 41: Evolution of model surface pressures in three selected stress points during the foundation installation (Phase 2)

The effect of wetting is first analysed when the water table is increased by 2m.

In this scenario, the unsaturated zone reduces (wetting), and the new distribution of suction is shown in Figure 42 (on page 48). Due to this wetting phase, irreversible displacements are observed below the foundation. Figure 43 (on page 48) shows the phase displacement in vertical direction at the end of Phase 3, with a maximum of about 2.5 cm below the foundation.

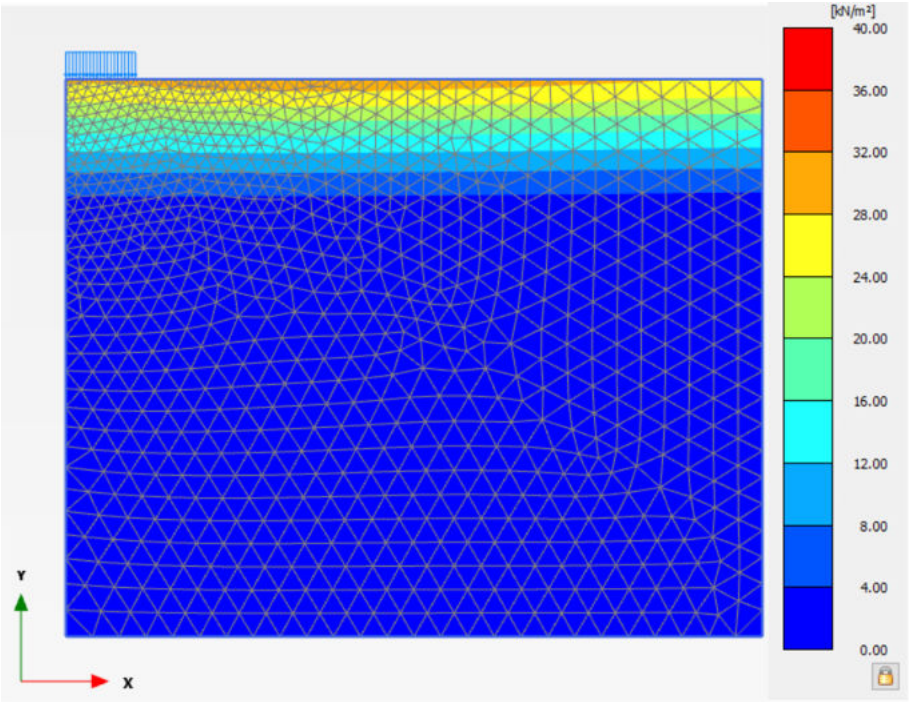

Figure 42: Suction distribution at the end of the water table raising phase (Phase 3)

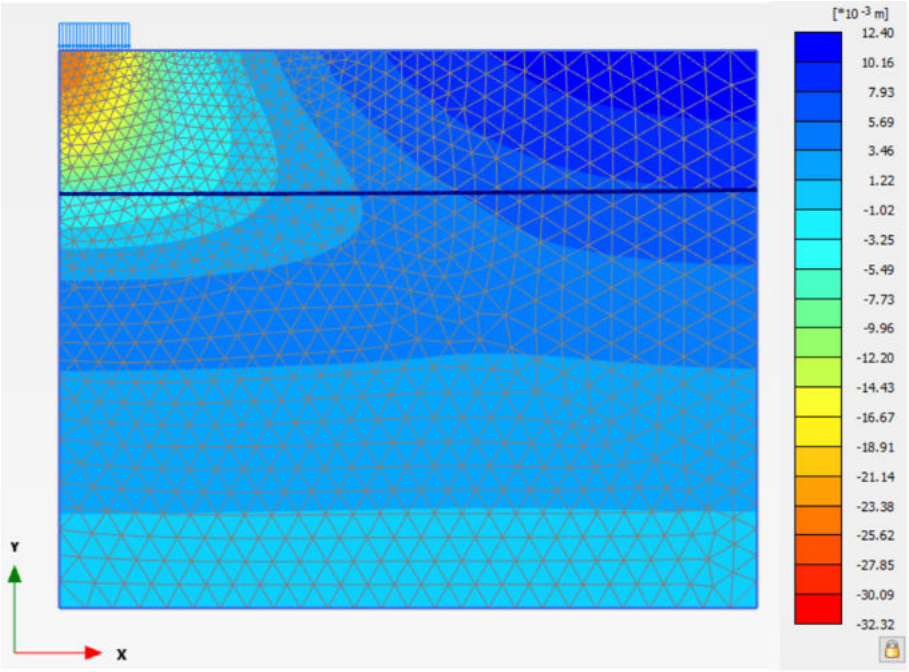

Figure 43: Vertical phase displacement at the end of Phase 3

Just below the foundation (Stress point N) (Figure 44 (on page 49)), suction remains initially constant as the effect of the water table change becomes more visible after 30 days. This process is accompanied by plastic strains as $p_0{}'$ slowly increases although still remaining distinct from $p_c{}'$.

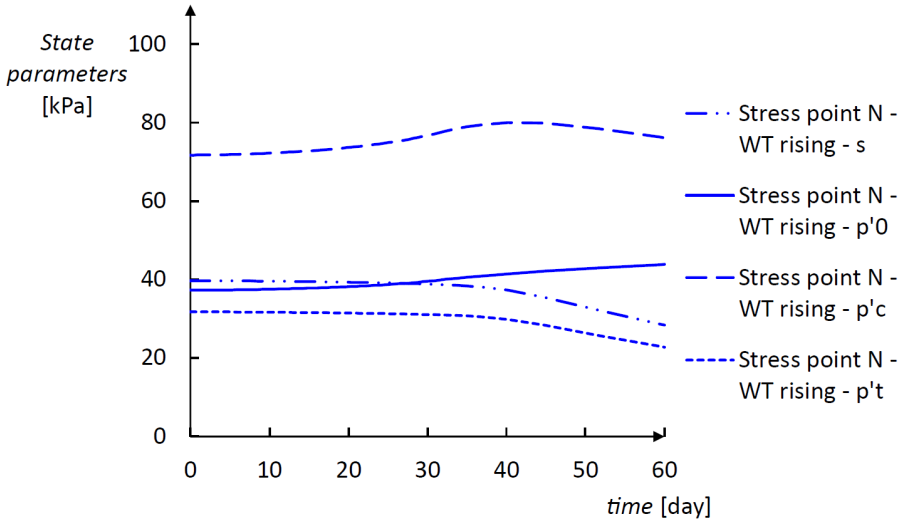

Figure 44: Evolution of suction and model surface pressures in the stress point just below the foundation, during the water table rising phase (Phase 3)

Instead, at a depth of 2m from the ground surface (Stress point O), a transition from an unsaturated state (suction equal to about 20kPa) to a fully saturated condition is observed (Figure 45 (on page 49)), with $p_0{}'$ and $p_c{}'$ converging to the same value while $p_t{}'$ tends to zero.

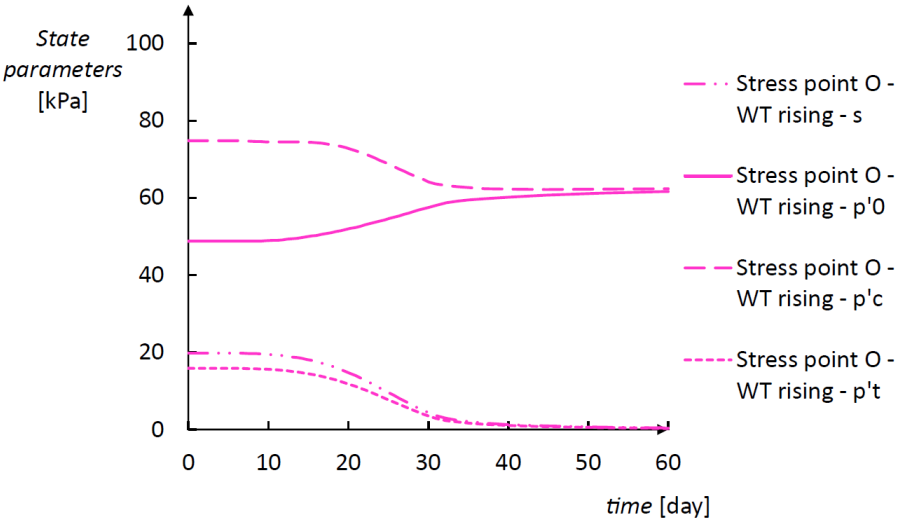

Figure 45: Evolution of suction and model surface pressures in the stress point at 2m depth from the foundation, during the water table rising phase (Phase 3)

At the ground surface, at a certain distance from the foundation (Stress point P), the reduction of suction occurs mostly within the elastic domain, as p_0' remains constant during the entire phase and p_c' decreases with suction (Figure 46 (on page 50)).

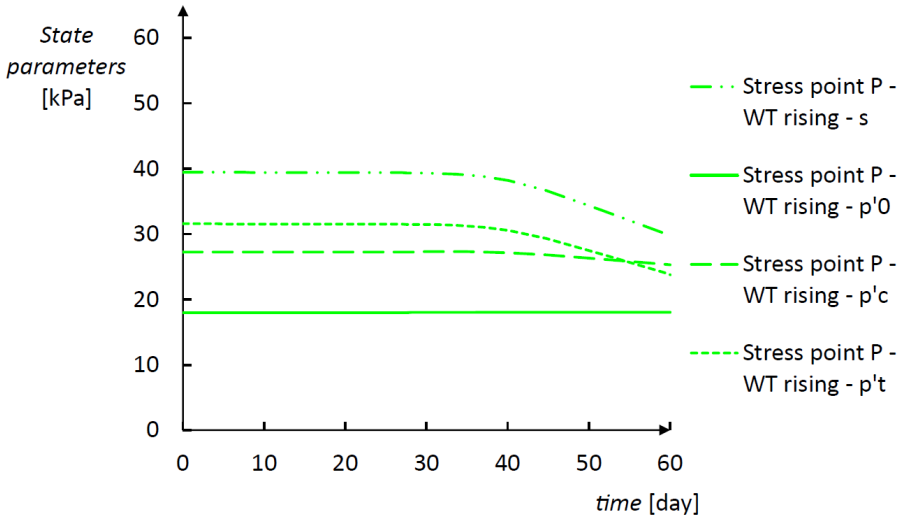

Figure 46: Evolution of suction and model surface pressures in the stress point at the ground surface, distant from the foundation, during the water table rising phase (Phase 3)

In the second scenario, when a precipitation event with the characteristics described above is simulated, the soil deposit behaves differently since suction starts decreasing at the top as water infiltrates in the ground and increases again when rain stops. Compared to the previous case, irreversible vertical phase displacements are higher with a maximum of about 3.3 cm (Figure 47 (on page 51)).

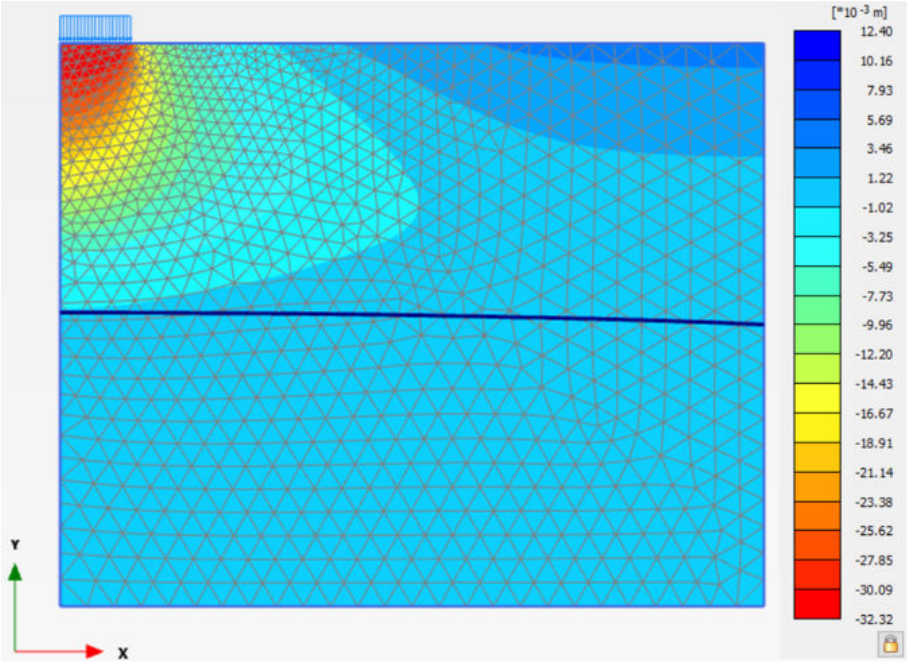

Figure 47: Vertical phase displacement at the end of Phase 4

The evolution of suction and the model surface pressures in the three selected points are shown in Figure 48 (on page 52), Figure 49 (on page 52) and Figure 50 (on page 53). In Stress point P, suction is equal to 40kPa at the beginning but decreases immediately to about 5kPa as an effect of water infiltration, Figure 50 (on page 53). Below the foundation (Stress point N), the change in suction is observed later, since no water can directly infiltrate there, due to the presence of the structure (simulated with a distributed load with a closed boundary, Figure 48 (on page 52)). Also at 2m depth (Stress point O), suction starts decreasing after 15 to 20 days of precipitation, as the water reaches that depth and moves down towards the water table, causing a slight increase in suction towards the end of the phase, as shown in Figure 49 (on page 52).

Away from the foundation, the stress state at the ground surface remains inside the elastic domain despite the change of suction, as $p_0{}'$ is generally constant. The first 30days correspond to a wetting phase, as suction reduces, while, when the precipitation stops, suction increases (drying).

In terms of vertical displacements (Figure 51 (on page 53)), three nodes close to the above mentioned stress points have been selected. At the end of the foundation installation, settlements have occurred in the three nodes, with different magnitude depending on the node location.

Below the foundation, both at the ground surface (Node A) and at 2m depth (Node B), the amount of settlement increases during both wetting phases, initially of a similar amount, but the difference becomes larger in the case of the precipitation after about 20days, showing (plastic) settlements.

At the ground level, distant from the foundation (Node C), the effect of swelling is immediately visible when the water infiltrates due to the precipitation, causing a reduction of the displacement in that node. However, when the precipitation stops and suction increases again, the soil contracts and settlements occur. The evolution of the vertical displacement is different when the water table raises, since the node is subjected to wetting only and, therefore, to swelling, with a slight decrease of u_y in that node.

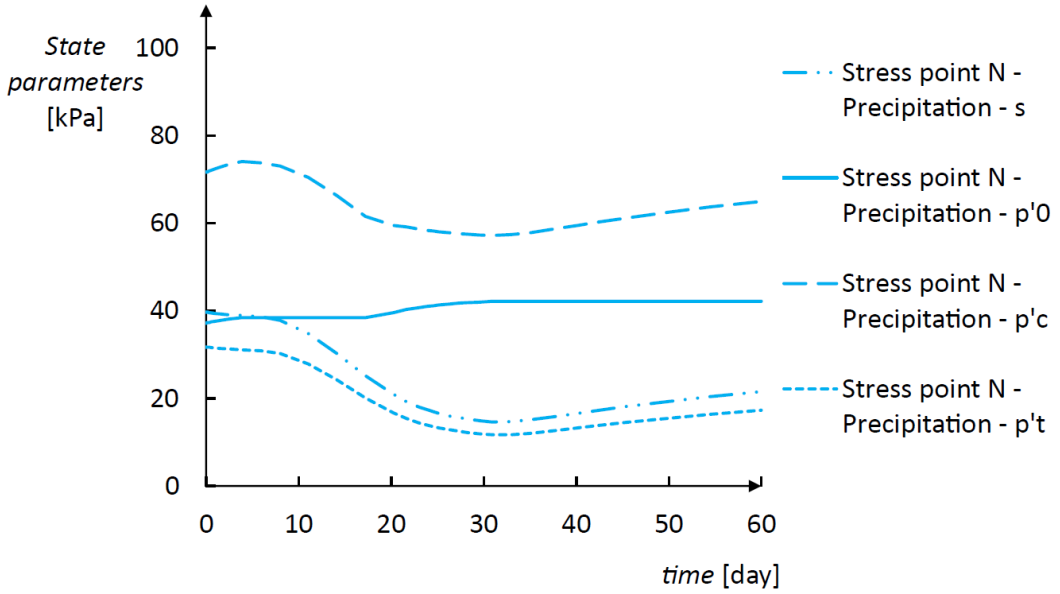

Figure 48: Evolution of suction and model surface pressures in the stress point just below the foundation, during the precipitation (Phase 4)

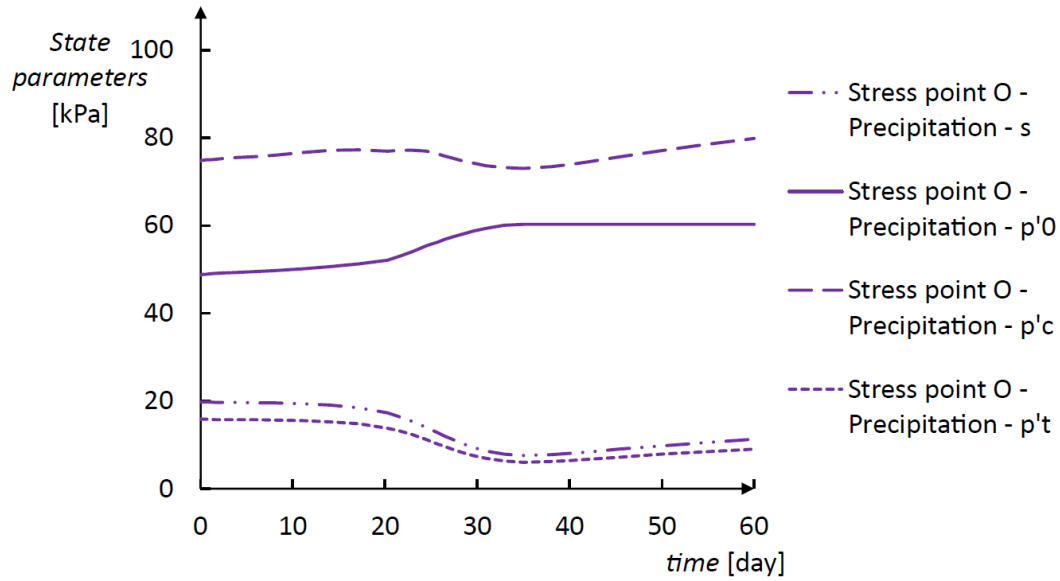

Figure 49: Evolution of suction and model surface pressures in the stress point at 2m depth from the foundation, during the precipitation (Phase 4)

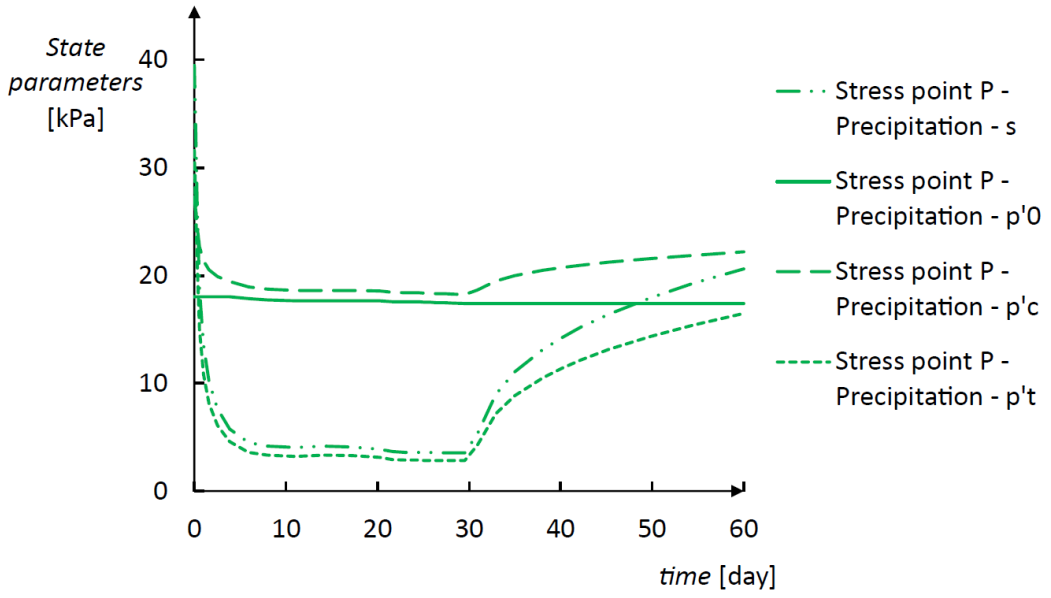

Figure 50: Evolution of suction and model surface pressures in the stress point at the ground surface, distant from the foundation, during the precipitation (Phase 4)

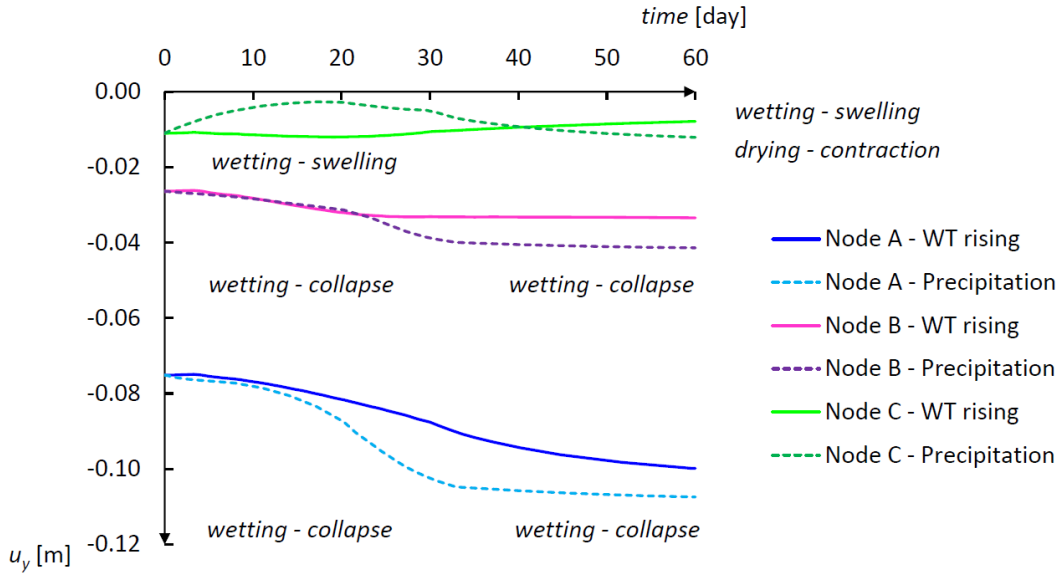

Figure 51: Evolution of vertical displacement in the three selected nodes, during the water table rising and precipitation phases

The analysis of the results shows that PLAXIS BBM can simulate the complex behaviour of soils subjected to drying and wetting phases, due to a change in the water level and, more in general, soil-atmosphere interaction.

6 References

1. Alonso, E. E., Gens, A., & Josa, A. (1990). A constitutive model for partially saturated soils. Géotechnique, 40(3), 405-430.
2. Bishop, A. W. (1959). The principle of effective stress. Teknisk ukeblad, 39, 859-863.
3. Bishop, A. W., & Blight, G. E. (1963). Some aspects of effective stress in saturated and partly saturated soils. Géotechnique, 13(3), 177-197.
4. Bolzon, G., Schrefler, B. A., & Zienkiewicz, O. C. (1996). Elastoplastic soil constitutive laws generalized to partially saturated states. Géotechnique, 46(2), 279-289.
5. Dudley, J. H. (1970). Review of collapsing soils. Journal of the Soil Mechanics and Foundations Division, 96(3), 925-947.
6. Fredlund, D. G., Morgenstern, N. R., & Widger, R. A. (1978). The shear strength of unsaturated soils. Canadian geotechnical journal, 15(3), 313-321.
7. Jaky, J. (1944) .The coefficient of earth pressure at rest. Journal of the Society of Hungarian Architects and Engineers, 355-358.
8. Jennings, J. E. B., & Burland,J. B.(1962). Limitations to the use of effective stresses in partly saturated soils. Géotechnique 12(2), 125-144.
9. Khalili, N., & Khabbaz, M. H. (1998). A unique relationship for χ for the determination of the shear strength of unsaturated soils. Géotechnique, 48(5), 681-687.
10. Mualem, Y. (1976). A new model for predicting the hydraulic conductivity of unsaturated porous media. Water resources research, 12(3), 513-522.
11. Ohmaki, S. (1982). Stress-strain behaviour of anisotropically, normally consolidated cohesive soil. Proc. 1st Int. Symp. Num. Mod. Geomech., Zurich, 250-269.
12. Pedroso, D. M., & Farias, M. M. (2011). Extended Barcelona basic model for unsaturated soils under cyclic loadings. Computers and Geotechnics, 38(5), 731-740.
13. Pereira, C. (2011). Study of the Barcelona Basic Model. Influence of suction on shear strength (Doctoral dissertation, Master Thesis, IST, Lisbon (in Portuguese)).
14. Roscoe, K. H., Schofield, A. N., & Wroth, C. P. (1958). On the yielding of soils. Géotechnique, 8(1), 22-53.
15. Roscoe, K. H., & Schofield, A. N. (1963). Mechanical behaviour of an idealised 'wet' clay. 2nd ECSMFE, Wiesbaden, 1, 47-54.
16. Schofield, A. N., & Wroth, C. P. (1968). Critical state soil mechanics. McGraw Hill, London, UK.
17. Sheng, D., Sloan S. W., & Yu H. S. (2000). Aspects of finite element implementation of critical state models. Computational mechanics 26(2), 185-196.
18. Van Genuchten, M. T. (1980). A closed-form equation for predicting the hydraulic conductivity of unsaturated soils. Soil science society of America journal, 44(5), 892-898.